TITLE

Spatial and temporal coordination of Duox/TrpA1/Dh31 and IMD pathways is required for the efficient elimination of pathogenic bacteria in the intestine of *Drosophila* larvae.

AUTHORS

Fatima Tleiss[1], Martina Montanari[2], Olivier Pierre[1], Julien Royet[2]*, Dani Osman[3]*, Armel Gallet[1]* and C. Léopold Kurz[2]*

AFFILIATIONS

1 : Université Côte d'Azur, CNRS, INRAE, ISA, France

2: Aix-Marseille Université, CNRS, IBDM, Marseille, France

3: UMR PIMIT (Processus Infectieux en Milieu Insulaire Tropical) CNRS 9192- INSERM 1187-IRD 249-Université de La Réunion, île de La Réunion, France.

* Corresponding authors: e-mail: armel.gallet@unice.fr; leopold.kurz@univ-amu.fr; dani.osman@univ-reunion.fr; julien.royet@univ-amu.fr

ABSTRACT

Multiple gut antimicrobial mechanisms are coordinated in space and time to efficiently fight foodborne pathogens. In *Drosophila melanogaster*, production of reactive oxygen species (ROS) and antimicrobial peptides (AMPs) together with intestinal cell renewal play a key role in eliminating gut microbes. An alternative protective mechanism would be to selectively prevent the penetration of the intestinal tract by pathogenic bacteria while allowing colonization by commensals. Using real-time imaging to follow the fate of ingested bacteria, we demonstrate that while commensal *Lactiplantibacillus plantarum* freely enter and cross the larval midgut, pathogenic strains such as. *Erwinia carotovora* or *Bacillus thuringiensis*, are actively locked down in the anterior midgut where they are rapidly eliminated by antimicrobial peptides. This sequestration of pathogenic bacteria in the anterior midgut requires the Duox enzyme in enterocytes, and both TrpA1 and Dh31 in enteroendocrine cells. Supplementing larval food with hCGRP, the human homolog of Dh31, is sufficient to trigger lockdown, suggesting the existence of a conserved mechanism. While the IMD pathway is essential for eliminating the trapped bacteria, it is dispensable for the lockdown. Genetic manipulations impairing bacterial lockdown results in abnormal colonization of posterior midgut regions by pathogenic bacteria. This ectopic colonization leads to bacterial proliferation and larval death, demonstrating the critical role of bacteria anterior sequestration in larval defense. Our study reveals a temporal orchestration during which pathogenic bacteria, but not innocuous, are compartimentalized in the anterior part of the midgut in which they are eliminated in an IMD pathway dependent manner.

AUTHOR SUMMARY

Typically, when considering the immune response of animals to infection, we focus on classical immunity, encompassing both innate and adaptive aspects such as antimicrobials and circulating immune cells. However, a broader perspective on immunity includes additional strategies that enhance host protection, such as behavioral avoidance and internal mechanisms that restrict pathogen propagation. In our study using *Drosophila* larvae as a model, we uncovered spatially and temporally interconnected events that are crucial for effectively combating intestinal infections. Our findings reveal a two-step defense mechanism: first, the larvae rapidly discriminate between bacterial strains, effectively confining hazardous ones in the anterior section of the intestine in a process we term 'lockdown'. These locked down bacteria trigger the synthesis and release of antimicrobial peptides by the host, which ultimately eradicate the entrapped pathogens. Our experiments show that larvae capable of both initiating a lockdown and producing antimicrobial peptides withstand infections. In contrast, the absence of either one of these sequential defenses results in high mortality among the larvae, emphasizing the importance of each step and the necessity of their precise coordination in the immune response.

58 **INTRODUCTION**

59 One of the key avenues by which bacterial pathogens infiltrate a host is through the ingestion
60 of contaminated food. If occurring, series of constitutive or inducible defense mechanisms
61 come into play to limit the infection and ideally eradicate the pathogens. These defenses
62 operate in a temporal manner, with mechanical and constitutive chemical barriers serving as
63 the first line of defense, followed by inducible mechanisms involving the production of
64 reactive oxygen species (ROS), the transcription, translation, and secretion of antimicrobial
65 peptides (AMPs) as well as inter-organ signaling to cope with possible upcoming stages of
66 infection. This temporality is evident between innate and adaptive immunity, with the former
67 considered the primary defense line that contains and combats the threat while preparing the
68 more subtle adaptive response.

69 To focus on deciphering innate immune processes, the insect *Drosophila melanogaster*
70 has been widely and successfully used (Neyen et al., 2014; Younes et al., 2020). This model
71 has made it possible to establish the chronology of the events involved in the defense against
72 pathogenic bacteria. In *Drosophila,* as in all metazoans, a layer made of mucus, completed
73 with a peritrophic membrane in insect midguts, protects the intestine lining from direct
74 contact with pathogens (Hegedus et al., 2009; Lemaitre and Miguel-Aliaga, 2013; Pelaseyed
75 et al., 2014). In adult *Drosophila*, a conserved immune response involving the production of
76 ROS by Duox (Dual oxidase) enzyme in enterocytes is triggered in the intestine as early as 30
77 minutes after ingesting pathogenic bacteria. ROS directly damage bacterial membranes
78 (Benguettat et al., 2018; Ha et al., 2009; Ha et al., 2005; Lee et al., 2013) but also exert an
79 indirect effect in adults by triggering visceral spasms through the host detection of ROS
80 mediated by the TrpA1 nociceptor and subsequent secretion of Diuretic Hormone 31 (Dh31)
81 by enteroendocrine cells (Benguettat et al., 2018; Du et al., 2016a). Dh31 then binds its

82 receptor on visceral muscles, triggering contractions that expedite bacterial elimination
83 (Benguettat et al., 2018). This pathway seems to be conserved during evolution as TrpA1 is a
84 *Drosophila* homolog of TRP receptors that respond to noxious conditions (Ogawa et al., 2016)
85 and Dh31 is the *Drosophila* homolog of the mammalian CGRP (Guo et al., 2021; Nässel and
86 Zandawala, 2019). In parallel, the IMD innate immune pathway is activated following bacterial
87 peptidoglycan detection, leading to the transcription AMP encoding genes and to the
88 subsequent secretion of the peptides that kill bacteria (Capo et al., 2016).

89 In this work, using *Drosophila* larvae, we developed a real-time experimental system
90 to trace the fate of pathogenic bacteria ingested with food. We characterized a new
91 mechanism implicated in the lockdown and elimination of pathogenic bacteria in the anterior
92 part of the midgut. We demonstrated that this lockdown is regulated by the ROS/TrpA1/Dh31
93 axis. Our results delineate a model in which bacterial trapping arises from ROS production in
94 the intestinal lumen in response to pathogenic bacteria. These ROS compounds interact with
95 TrpA1 in Dh31-expressing enteroendocrine cells located between the anterior and middle
96 midgut, leading to Dh31 secretion and subsequent bacterial lockdown, suggesting the closure
97 of a pylorus-like structure. Interestingly, we found that human CGRP can replace Dh31 in
98 inducing the trapping of bacteria or fluorescent particles. Our findings also highlight the
99 central role of this blockage, which acts first allowing sufficient time for the subsequent
100 eradication of trapped pathogens by the IMD pathway and its downstream effectors.
101 Collectively, our data unravel a finely tuned coordination between the ROS/TrpA1/Dh31 axis
102 and the IMD pathway, enabling an effective bactericidal action of AMPs.

103

104 **RESULTS**

105 **Bacterial lockdown in the anterior part of larval intestine**

106 The translucency of *Drosophila* larvae allows for live studies of immune defense components
107 and their coordination in eradicating pathogenic bacteria. Previously, we reported a decrease
108 in food intake in larvae exposed to contaminated food with the Gram-negative opportunistic
109 bacterium *Erwinia carotovora carotovora* (*Ecc15*), a process involving TrpA1 (Keita et al.,
110 2017). Using blue food dye, we tracked food intake and observed that larvae remained blue
111 without bacterial contaminants, while in the presence of *Ecc15*, they appeared clearer,
112 indicating reduced food intake (Keita et al., 2017). Such a strategy was already used to identify
113 a food-uptake cessation for larvae orally infected by *Pseudomonas entomophila* (Liehl et al.,
114 2006). However, the assay with *Ecc15* was limited to 1h post-ingestion and using a food dye,
115 not directly monitoring the fate of the ingested bacteria over the time. We therefore designed
116 a protocol allowing to film the fate of fluorescent bacteria once ingested by the larvae. We
117 tested three different fluorescent bacteria: *Ecc15-GFP* (*Ecc*), *Bacillus thuringiensis-GFP* (*Bt*, an
118 opportunistic Gram-positive bacterium) and *Lactiplantibacillus plantarum-GFP* (*Lp*, a
119 commensal Gram-positive bacterium). After 1 hour of feeding on contaminated media, *Ecc*
120 and *Bt* were concentrated in the anterior midgut (Movies 1 and 2). The location of the bacteria
121 specifically in the anterior part of the intestine following 1h exposure was confirmed when
122 individuals from populations were imaged and counted (Fig 1A). Remarkably, tracking the GFP
123 signal over time revealed that it remained in the anterior part of the larva and began to fade
124 6 hours after ingestion (Movies1 and 2; SUPP1A and SUPP1B). This fading suggests the
125 elimination of the bacteria, while the larva continued to exhibit active movements. This
126 pattern was observed for both *Ecc* and *Bt*. However, unlike the opportunistic bacteria *Ecc* and

127 *Bt*, *Lp* was present in the posterior compartment of the larval midgut after 1 hour of feeding
128 and remained there throughout the 16-hour duration of our observation (Movie 3, Fig 1A and
129 SUPP1C) (Storelli et al., 2018). To better characterize the lockdown phenomenon, we counted
130 the ratio of larvae with trapped GFP-bacteria 1h post feeding. We found that more than 80%
131 of the larvae had *Ecc* and *Bt* bacteria localized in the anterior part of the midgut (Fig 1A and
132 1B). The portion of the intestine containing the fluorescent bacteria is delimited posteriorly
133 by an extensive turn. To confirm our findings, we dissected the intestines of larvae that had
134 ingested the bacteria. Our analysis confirmed that *Ecc* and *Bt* were predominantly located in
135 the anterior part of the intestines, whereas *Lp* was not, supporting our initial observations
136 (SUPP2A). Our data collectively indicate that pathogenic bacteria, such as *Ecc* and *Bt*, are
137 spatially confined to the anterior part of the larval midgut before their disappearance. In
138 contrast, the commensal bacterium *Lp* is distributed throughout the midgut, persisting
139 principally in the posterior part. This distinction underscores the different interactions and
140 survival strategies of pathogenic versus commensal bacteria within the larval midgut.

141 **The anterior intestinal localization of pathogenic bacteria is dose-specific and occurs rapidly**

142 We hypothesized that the bacteria lockdown in the anterior part of the larval intestine was an
143 active host response and might be dependent on the bacterial dose. To test this, we exposed
144 larvae to varying concentrations of *Ecc* and *Bt* and measured the lockdown ratio. We found
145 that a concentration of 2.10^9 *Ecc* bacteria per ml was sufficient to induce lockdown, whereas
146 for Bt, a higher concentration of 4.10^{10} *Bt* bacteria per ml was required (Fig 2A). This dose-
147 dependent result with *Ecc* eliciting the lockdown at a tenfold lower bacterial count than *Bt*,
148 aligns with our previous findings that *Ecc* is more virulent than *Bt* in the *Drosophila* adult
149 intestine (Loudhaief et al., 2017). In order to ascertain whether the bacterial concentrations

150 employed in our experiments could be representative of those encountered by larvae in the
151 absence of human manipulation, we assessed bacterial concentrations within 1 mm-sized
152 colony for both *Ecc* and *Bt* on LB agar plates. The average optical density at 600 nm (OD_{600}) for
153 these colonies was 31 for *Ecc* and 19.3 for *Bt*, corresponding to approximately 15 10^{10} *Ecc*
154 bacteria per mL and 2.8 10^{10} *Bt* bacteria per ml (data can be found in the source data file).
155 These values are consistent with the doses required in our assays to induce the lockdown
156 phenomenon (Fig 2A). For all subsequent experiments, we used 4.10^{10} bacteria per ml.

157 In previous intoxication assays, we arbitrary used a 1-hour time point to assess the
158 phenotype. However, observations of lockdown occurring within minutes suggested that this
159 response does not require *de novo* protein synthesis by the host. Shorter exposure times
160 revealed that *Ecc* was blocked in the anterior part of the intestine within 15 minutes, while *Bt*
161 showed a similar pattern beginning at 15 minutes and completing by 30 minutes (Fig 2B and
162 2C). Again, although lockdown was observed with both *Ecc* and *Bt*, *Ecc* proved to be more
163 potent in inducing this response. Based on these results, we defined 1h as our standard
164 exposure time of larvae with bacterial contaminated food.

165 Our assays typically involved groups of approximately 50 larvae to observe population-
166 level phenomena. Recent studies have suggested that larval behavior can be influenced by
167 group dynamics (Dombrovski et al., 2019; Dombrovski et al., 2017; Louis and de Polavieja,
168 2017; Mast et al., 2014). To determine whether group size affected the lockdown response,
169 we exposed groups of varying sizes to *Bt* or *Ecc* and measured the lockdown ratio. The
170 phenomenon proved robust even with a single larva exposed to contaminated food, indicating
171 that the response was not influenced by group size under our experimental conditions (Fig

172 2D). Based on these findings, for all subsequent experiments, we standardized the conditions
173 using 4.10^{10} bacteria per ml, a 1-hour exposure time, and groups of at least 20 larvae.

174 **Host TrpA1 and Dh31 are crucial for the lock down phenotype**

175 In our previous study on larval intake of food contaminated with *Ecc* (Keita et al., 2017), we
176 identified the gene *TrpA1* as essential in the host. The TrpA1 protein, a member of the TRP
177 channel family, facilitates Ca2+ entry into cells at temperatures over 25°C or upon exposure
178 to chemicals such as ROS (Du et al., 2016b; Gu et al., 2019; Guntur et al., 2015). This channel,
179 recognized as a nociceptor (Lapointe and Altier, 2011), has been linked to intestinal muscle
180 activity in adult *Drosophila* following *Ecc* exposure (Du et al., 2016a) and in response to ROS
181 production by the host (Benguettat et al., 2018). We examined the role of TrpA1 during the
182 larval response to contaminated food using *TrpA1*$^{[1]}$ homozygous viable mutant in an
183 experimental setup with fluorescent *Lp*, *Ecc* or *Bt* bacteria. In this mutant larvae, while the
184 localization of *Lp* in the posterior midgut remained unchanged, *Ecc* and *Bt* failed to be confined
185 into the anterior midgut and were instead found in the posterior midgut. (Fig 3A, 3B, movie 4
186 and SUPP3A). This observation underscores that TrpA1 is necessary for the lockdown of
187 pathogenic bacteria in the anterior midgut. Considering previous reports on visceral
188 contraction in adult *Drosophila* involving ROS production, detection by TrpA1, and Dh31
189 secretion to expel bacteria (Benguettat et al., 2018; Du et al., 2016a), we wondered whether
190 a similar ROS/TrpA1/Dh31 signaling axis is necessary in larvae to block pathogenic bacteria in
191 the anterior midgut. Indeed, though the bacterial lockdown we observed did not expel
192 microorganisms, it might involve muscle contractions triggered by the food contamination.
193 Thus, we tested the lockdown ratio of *Dh31*$^{[KG09001]}$ homozygous viable mutants (*Dh31*$^{-}$)
194 exposed to *Lp*, *Bt* or *Ecc* bacteria. In contrast to control animals, where fewer than 20% of

195 larvae exhibited *Ecc* or *Bt* in the posterior section of the intestine, for more than 60% of *Dh31*$^{-}$
196 mutant larvae, the pathogenic bacteria *Bt* or *Ecc* were localized in the posterior midgut
197 confirming Dh31's crucial role in this mechanism (Fig 3A and 3B, movie 5 and SUPP3B). The
198 localization of *Lp* was not affected (Fig 3B). The human Calcitonin Gene-Related Peptide
199 (hCGRP) is the functional homolog of Dh31. Indeed, hCGRP has been shown to promote
200 visceral muscle contractions in adult flies (Benguettat et al., 2018). To investigate whether the
201 lockdown could be triggered without pathogenic bacteria in response to a hormone, we
202 exposed larvae to either *Lp* or Dextran-FITC in the presence of hCGRP. While *Lp* and Dextran-
203 FITC were normally distributed throughout the midgut, adding hCGRP to the food induced a
204 significant lockdown (Fig 3B and 3C and movie 6). Interestingly, *Lp* locked down in the anterior
205 midgut due to hCGRP began to be released after 6 hours (movie 6 and SUPP3), suggesting a
206 dynamic and reversible phenomenon, likely linked to Dh31/hCGRP hormone metabolization.
207 This demonstrates that the process could be triggered independently of the bacteria by a
208 hormone, highlighting it as an active host mechanism.

209 **Duox in Enterocytes and Dh31 in Enteroendocrine cells control pathogenic bacteria**

210 The activation of TrpA1, potentially leading to the release of Dh31, (Belinskaia et al., 2023;
211 Kondo et al., 2010; Kunst et al., 2014) could be a consequence of ROS production in the host
212 larval midgut in response to *Ecc* or *Bt*. The larval intestine comprises two main cell populations:
213 enterocytes (ECs) and enteroendocrine cells (EECs). In adult *Drosophila*, Dh31 is stored in EECs
214 and is secreted in response to TrpA1 activation, a process well documented in literature
215 (Benguettat et al., 2018; Chen et al., 2016; Veenstra et al., 2008). The role of ROS in the
216 immunity of adult *Drosophila* intestine following infection has also been reported (Chakrabarti
217 et al., 2012; Ha et al., 2005; Lee et al., 2013; Ryu et al., 2006). To investigate the involvement

218 of ROS in the larval bacterial lockdown, we focused on Duox, the primary enzyme responsible
219 for luminal ROS production. We spatially silenced *Duox* expression using RNA interference
220 (*UAS-Duox_IR*) driven by an ubiquitous driver (Da-Gal4), a driver specific of ECs (Mex-Gal4) or
221 an EECs specific driver (Pros-Gal4). In parallel, using the same set of drivers, we tested the
222 effects of cell-autonomous *Dh31* silencing using RNAi (*UAS-Dh31_IR*). Upon exposing these
223 larvae to a food mixture contaminated with fluorescent *Ecc* or *Bt*, we assessed the lockdown
224 ratio. Our results indicate that in larvae, Duox is essential in ECs for the lockdown of both *Ecc*
225 and *Bt* (Fig 3D). Furthermore, silencing *Dh31* in EECs not only confirmed the mutant phenotype
226 but also indicated that Dh31, necessary for the lockdown, is produced by EECs (Fig 3D). This
227 data underscores the pivotal roles of Duox in ECs and Dh31 in EECs for the entrapment of
228 pathogenic bacteria in the anterior part of the *Drosophila* larval midgut.

229 **Absence of ROS prevents lockdown phenotype and leads to larval death**

230 Our data demonstrating that Duox protein is necessary for the lockdown phenotype, implies
231 that ROS generated by this enzyme are critical. The involvement of TrpA1, a known ROS
232 sensor, further highlights the significance of these compounds in the process. To corroborate
233 the necessity of ROS, we neutralized luminal ROS using DTT (Dithiothreitol), a potent reducing
234 agent known for its efficacy against ROS, mixing it with the larval food (Benguettat et al.,
235 2018). In normal conditions, larvae fed with *Bt* exhibit a lockdown of the bacteria in the
236 anterior part of their intestine, as shown previously in FIG 1A, 1B and Fig 4A. However, when
237 the larvae were exposed to a mixture of *Bt* and DTT, the intestinal lockdown of bacteria in the
238 anterior midgut was abolished (Fig 4A). The effect of DTT over the lockdown phenotype was
239 quantified using DTT mixed to Dextran-FITC in order to compare with a condition leading to
240 an almost full posterior localization (FIG 4B). Together our results strongly suggest that the

241 role of Duox enzyme in producing ROS in the larval intestine is crucial, and these ROS act as
242 key signals initiating the lockdown mechanism.

243 **The lockdown is crucial for bacterial elimination and larval survival**

244 Our real-time observations showed that between 6 and 8 hours after the lockdown of *Bt* or
245 *Ecc* in the anterior midgut, the bacteria disappeared (movies 1 and movie 2, SUPP1A and
246 SUPP1B). This led us to investigate the relationship between pathogen localization and larval
247 survival. The hypothesis was that the disappearance of the GFP signal corresponded to the
248 bacterial death. We therefore assessed the *Lp*, *Bt* or *Ecc* load over time in dissected midguts
249 of control larvae previously exposed to contaminated food. Consistent with our film data,
250 while the *Lp* load remained stable, the quantities of *Ecc* and *Bt* diminished rapidly in the
251 intestines of control larvae, with no bacteria detectable 8 hours post-ingestion and lockdown
252 (Fig 5A, 5B and 5C). However, in the intestines of *TrpA1*$^{[1]}$ and *Dh31*$^{-}$ mutants, the amount of
253 *Bt* and *Ecc* increased overtime (Fig 5B and 5C). Unfortunately, we were unable to assess the
254 bacterial load beyond 6 hours due to the deterioration of the midguts. Supporting this, in
255 movies 4 and 5 (SUPP3A and SUPP3B), we observed that *Bt* or *Ecc* bacteria which were not
256 locked down in the anterior part of the midgut did not disappear over time. More importantly,
257 *TrpA1*$^{[1]}$ and *Dh31*$^{-}$ mutant larvae containing *Bt* or *Ecc* stopped to move suggesting they were
258 dead. We confirmed the precocious death of the *TrpA1*$^{[1]}$ and *Dh31*$^{-}$ larvae fed with either *Bt*
259 or *Ecc* compared to control animals (Fig 5D and 5E). Importantly, these mutants exhibited
260 sustained viability overnight when fed with a mixture containing *Lp* or a bacteria-free diet (Fig
261 5E). Interestingly, control larvae fed a mixture of *Bt* and DTT, which neutralizes ROS and thus
262 inhibits the lockdown, also perished (Fig 5F). This mortality was not due to DTT, as larvae fed
263 Dextran-FITC plus DTT survived (FIG 5F). These findings suggest that, in larvae, the active

264 lockdown of *Bt* and *Ecc* in the anterior part of the midgut – involving a sequence of events
265 with ROS production by Duox, TrpA1 activation by ROS, and Dh31 secretion – is essential for
266 bacterial elimination by the host. Thus, failure to lock down pathogenic bacteria like *Ecc* or *Bt*
267 results in their proliferation and consequent larval death.

268 **The lockdown area is delimited by TRPA1+/Dh31+ cells and muscular structures**

269 The above results suggest a working model involving the ROS/TrpA1/Dh31 axis in which Dh31
270 release from EECs leads to muscle contractions. However, unlike in adult *Drosophila*, where
271 bacteria are expelled from the gut, in larvae, we observed a blockade mechanism. To better
272 understand the physiology of the process, we utilized confocal microscopy to thoroughly
273 examine larval midguts and explore the relationship between TrpA1-positive (TrpA1+) cells,
274 anterior lockdown of the bacteria, and muscular structures. In larval midguts, TrpA1+ cells
275 were also Dh31+, and these Dh31+ cells were identified as EECs (Pros+), typically located at
276 the end of the anterior midgut. With the reporter line we used (*TrpA1*-Gal4/UAS-RFP), we
277 noted an average of 3 TrpA1+/Dh31+ cells per gut (ranging from 2 to 6 cells across 14
278 examined guts, see source data file) (Fig 6A-6F). This observation was in agreement with our
279 genetic and functional data linking Dh31 with EECs (FIG 3D) and suggested that TrpA1 and
280 Dh31 operate within the same cells (Fig 6C, 6C' and 6C''). The shape of these TrpA1+ Dh31+
281 cells was characteristic of EECs (Fig 6A'). In agreement with a model involving an interaction
282 of secreted ROS with TrpA1 and a subsequent local Dh31 release to act on muscles, following
283 exposure to food contaminated with fluorescent *Bt* or *Ecc*, the bacteria were locked down in
284 an area delimited by the anterior part of the gut and the TrpA1+ cells patch (Fig 6B).
285 Additionally, we observed that the amount of Dh31 within Pros+ cells of larvae blocking
286 bacteria was lower compared to those not exhibiting the lockdown, such as *TrpA1* mutant (Fig

287 6D and 6E). Then, we wondered whether specific muscle structures would exist close to the
288 TrpA1+ cells in the anterior midgut. Actin labeling revealed fibrous structures on the basal side
289 of the gut and attached to it in a transversal position (Fig 6C'' and 6F-6H'). These structures,
290 typically lost during dissection, have been described in a report studying larval midgut
291 peristalsis (LaJeunesse et al., 2010). Notably, the attachment points of these filaments, or
292 tethers, corresponded with the locations of TrpA1+ cells and the boundary of the area where
293 *Ecc* or *Bt* were confined (Fig 6C'' and 6F-H). These filaments have been described as
294 longitudinal muscles emanating from two out of the four gastric caeca, but this might be a
295 misinterpretation of the images generated by Lajeunesse et al. (2010). Indeed, a recent study
296 describes these muscular structures using *in vivo* observations without dissections.
297 Interestingly, they show that these muscles belong to a subgroup of alary muscles named
298 TARMs (Thoracic Alary Related Muscles) (Bataillé et al., 2020). Specifically, TARMsT1 connect
299 the anterior of the larvae to the extremities of gastric caeca, while TARMsT2 link the anterior
300 part of the gut to the larval epidermis. Our findings support the hypothesis that the observed
301 muscular structures close to the TrpA1+ cells are TARMsT2 (Fig 6C'', 6F-6H', SUPP 4 and movie
302 7). These TARMsT2 are attached to the longitudinal gut muscles and the intestine forms a loop
303 at the attachment site (Fig 6H' and SUPP4)(Bataillé et al., 2020). The presence of Dh31+ EECs
304 in this specific curved region of the gut close to the TARMsT2 attachment (Fig 6C'') along with
305 our genetic and functional data lead to the hypothesis that this region may display a pyloric-
306 like activity triggered by Dh31 (and also hCGRP) following exposure to pathogenic bacteria.

307 **IMD pathway is mandatory for eliminating trapped bacteria**

308 In our study, we observed that control larvae were able to kill *Ecc* and *Bt* bacteria trapped in
309 the anterior part of the gut within 6-8 hours (movies 1 and 2 and Fig 5A-C). This finding raised

310 questions about the mechanism of bacterial elimination and the potential role of the IMD
311 (Immune Deficiency) pathway in this process. While larval intestinal immunity is multifaceted,
312 a key defense mechanism against bacteria is the production and secretion of AMPs (Hanson
313 and Lemaitre, 2020). Previous studies have reported the production of ROS in larval guts, but
314 this has not been directly linked to the killing of bacteria (Wu et al., 2012). In addition, we have
315 previously shown in adult *Drosophila* that ROS on their own are not sufficient to kill bacteria
316 (Benguettat et al., 2018). Thus, we focused our investigations on AMPs. Both *Ecc* and *Bt*
317 possess DAP-type peptidoglycans (PGN), known to activate the IMD signaling cascade, which
318 leads to the production of AMPs like Diptericin (Kaneko et al., 2006; Leulier et al., 2003;
319 Stenbak et al., 2004). We used various mutants deficient in components of the IMD pathway,
320 including PGRP-LC and PGRP-LE (PGN receptors), Dredd (an intracellular component), and
321 Relish (a NF-κB transcription factor) (Zhai et al., 2018). Additionally, we studied a mutant,
322 *ΔAMP14*, lacking 14 different AMPs (Carboni et al., 2022). We first assayed whether the IMD
323 pathway was required for the lockdown phenotype upon ingestion of *Bt* or *Ecc*. While *Lp* was
324 distributed throughout the gut of IMD pathway mutants, *Ecc* and *Bt* were confined to the
325 anterior part of the intestine, akin to control larvae (movies 8-12, SUPP5 and SUPP6 and Fig
326 7A and 7B). Thus, the IMD pathway is not required for the lockdown of *Ecc* and *Bt* in larval
327 intestines. Nevertheless, the movies suggested a death of the IMD mutant larvae despite the
328 lockdown of either *Bt* or *Ecc*. We therefore tested the survival of these IMD pathway mutants
329 following a 1h feeding with a mixture containing or not (water) fluorescent bacteria. While
330 neither control animals nor the IMD pathway mutants died following a 1h feeding period with
331 a *Lp* contaminated or non-contaminated food, all the IMD pathway mutants, including
332 *ΔAMP14*, had a decreased survival after exposure to *Ecc* or *Bt* (Fig 7C and 7D). Thus, the IMD
333 pathway is central for the survival of these animals with locked down bacteria in the anterior

334 part of the intestine. As this increased lethality in IMD pathway mutants might be related to
335 an uncontrolled growth of the locked down *Bt* and *Ecc* bacteria, we performed CFU counting.
336 With *Bt* and *Ecc*, while the initial inoculum was divided by 10^3 in 8h in the control larvae, the
337 bacterial population was maintained and even increased 10-fold in IMD pathway mutants
338 including *ΔAMP14* (Fig 7E and 7F). Additional observations from filming the fate of *Bt* and *Ecc*
339 in IMD pathway mutant larvae confirmed these findings (movies 8-12). The GFP-bacteria,
340 although locked down in the anterior part of the intestine, did not disappear, coinciding with
341 larval immobility and presumed death. In conclusion, our findings illustrate that although the
342 IMD pathway is dispensable for the initial sequestration of pathogenic bacteria, a process
343 contingent on the ROS/TrpA1/Dh31 axis, it plays a crucial role in their subsequent elimination.
344 Indeed, the AMPs produced following IMD pathway activation are essential for killing the
345 trapped bacteria and ensuring larval survival (Figure 8).

346

347

348 **DISCUSSION**

349 Leveraging the transparency of the *Drosophila* larvae, we have successfully developed
350 a novel real-time experimental system to monitor the fate of fluorescent bacteria ingested
351 along with food. This methodological advancement has enabled us to unveil a previously
352 uncharacterized physiological pathway necessary for the efficacy of the larval intestinal
353 immune response, specifically involving enteroendocrine cells. Our research has uncovered a
354 unique defense mechanism centered around a pylorus-like structure located in the anterior
355 midgut, regulated by the enteroendocrine peptide Dh31. Notably, we observed that
356 pathogenic bacteria, encompassing both Gram-positive and Gram-negative types, were
357 confined to the anterior section of the larval intestine as early as 15 minutes post-ingestion.
358 We determined that this intestinal lockdown of pathogenic bacteria necessitates a
359 ROS/TrpA1/Dh31 axis initiated by Duox activity in enterocytes in response to pathogenic
360 bacteria. We suspect the secrted ROS to interact with the TrpA1 ion channel receptor located
361 in Dh31-expressing enteroendocrine cells adjacent to the pylorus-like structure (Figure 8).
362 Previous studies on the interaction between ROS and TrpA1 support our hypothesis (Ogawa et
363 al., 2016). The confining of pathogenic bacteria to the anterior part of the larval intestine is a
364 mandatory step prior to their subsequent elimination by the IMD pathway. Intriguingly,
365 previous studies utilizing fluorescent bacteria have already highlighted a specific localization
366 of pathogenic bacteria in the larval gut. Bacteria such as *Ecc15*, *Pseudomonas entomophila*,
367 *Yersinia pestis*, *Salmonella enterica serovar Typhimurium*, and *Shigella flexneri* were observed
368 predominantly in the anterior part of the larval gut 6 hours after oral infection (Basset et al.,
369 2000; Bosco-Drayon et al., 2012; Earl et al., 2015; Ramond et al., 2021; Vodovar et al., 2005).
370 Our findings suggest that these bacteria can all induce ROS production by enterocytes,
371 providing a unifying mechanism for their containment and elimination in the larval gut.

372 Interestingly, it has been reported that the opportunistic pathogen *Staphylococcus aureus*
373 *(strain USA300)* predominantly colonizes the posterior midgut of *Drosophila* larvae, leading to
374 the death of 93% of the larvae (Ramond et al., 2021). This strain of *S. aureus* produces high
375 levels of detoxifying enzymes, such as catalase and superoxide dismutases, which effectively
376 neutralize ROS. The authors suggested that the neutralization of ROS bactericidal activity by
377 these enzymes is directly responsible for the bacterial proliferation and consequent host
378 mortality (Ramond et al., 2021). However, considering our findings, we propose an alternative
379 interpretation: the neutralization of ROS by these detoxifying enzymes might prevent the
380 closure of the pylorus, thereby allowing *S. aureus* to access and establish in the posterior
381 midgut. Our data also indicate that when pathogenic bacteria reach the posterior midgut, as
382 observed in larvae fed with DTT or in *TrpA1* or *Dh31* mutants, larval survival is significantly
383 jeopardized. This suggests that larval mortality could be attributed not to the inhibition of ROS
384 in the posterior midgut but rather to the presence of bacteria in this region. In the study
385 Ramond and colleagues (2021) involving *S. aureus*, the observation of bacterial spread into the
386 posterior part was recorded 3 hours post-infection. It would be insightful to further investigate
387 the dynamics of bacterial diffusion to determine whether, like other pathogens we studied, *S.*
388 *aureus* is initially confined to the anterior part of the gut shortly after ingestion, specifically
389 around 15 minutes post-infection. This could provide a broader understanding of the interplay
390 between pathogen-specific strategies and host defense mechanisms in *Drosophila* larvae.

391 Our study has focused on an elbow-shaped region in the *Drosophila* larval midgut,
392 characterized by a narrowing of the lumen and surrounded by muscular fibers. This region,
393 where we observed a halt in transit when food is contaminated, has been aptly termed a
394 pylorus-like due to its functional similarity to the human pyloric region. Interestingly, Bataillé
395 et al. (2020) reported the presence of muscular fibers in this area that are part of a subgroup

396 of alary muscles known as TARMs (Thoracic Alary Related Muscles). Specifically, TARMsT1
397 connect the anterior part of the larvae to the extremities of a pair of gastric caeca, whereas
398 TARMsT2 link the anterior part of the intestine to the larval epidermis. Our actin staining
399 corroborates the identification of these muscles as TARMsT2, which are attached to the
400 longitudinal muscles of the intestine, causing the intestine to form a loop at the site of
401 attachment (Bataillé et al., 2020). The presence of Dh31-positive enteroendocrine cells (EECs)
402 in this specific elbow-shaped region, close to the TARMsT2 attachment point, combined with
403 our genetic and functional data, supports the hypothesis that this region exhibits pyloric-like
404 activity. This activity is likely triggered by Dh31 or human Calcitonin Gene-Related Peptide
405 (hCGRP) following bacterial exposure. Notably, our previous research in adult *Drosophila*
406 showed that Dh31/hCGRP secretion induces contractions of the visceral longitudinal muscle
407 fibers, expelling pathogenic bacteria rapidly (Benguettat et al., 2018). However, in larvae,
408 while Dh31/hCGRP likely induces muscle contractions, the ensuing action may manifest as the
409 closure of a pylorus, as evidenced by the observed retention of pathogenic bacteria.
410 Importantly, in both larvae and adults, the same pathway and type of muscle fibers appear to
411 be involved, as TARMsT2 are connected to longitudinal fibers (Figure 6H') (LaJeunesse et al.,
412 2010). This finding is significant as it illustrates a conserved mechanism across developmental
413 stages, albeit with different outcomes: expulsion of pathogens in adults and containment in
414 larvae. In both cases, the overarching objective is the effective elimination of pathogens,
415 demonstrating the versatility and adaptability of the *Drosophila* immune response.

416 Hence, our work shed lights on a yet to be anatomically characterized pylorus-like
417 structure within the *Drosophila* larval gut, presenting a potential model for studying the
418 functions and roles of mammalian pylori. Notably, CGRP (Calcitonin Gene-Related Peptide)
419 secreting enteroendocrine cells have been identified in the mammalian pylorus, as highlighted

420 in research by (Kasacka, 2009) and (Bulc et al., 2018). Drawing parallels with mammalian
421 stomachs, the pylorus is typically closed, opening only when the stomach becomes full. In
422 exploring the functionality of the *Drosophila* pylorus-like, we considered two hypotheses: one,
423 where it operates similarly to its mammalian counterpart, closing by default and opening in
424 response to a full stomach, and another, where it remains open by default and closes upon
425 detection of infected food in the intestine. Our observations with the commensal bacteria *Lp*
426 (movie 3) suggest an initial closure of the pylorus as food accumulates in the anterior part of
427 the intestine, followed by its opening to allow the passage of non-pathogen-contaminated
428 food. This indicates a dynamic and responsive mechanism in the *Drosophila* gut. In contrast,
429 when *Drosophila* larvae encounter food contaminated with pathogenic bacteria, the pylorus
430 seems to contract, effectively blocking the passage of contaminated food into the anterior
431 part of the intestine. This finding is significant as it not only reveals a unique physiological
432 response in *Drosophila* larvae but also provides a basis for comparative studies with the
433 mammalian gastrointestinal system, particularly in understanding the regulatory mechanisms
434 governing pyloric function.

435 An intriguing question is why animals without a functional IMD pathway die from *Ecc*
436 or *Bt* exposure while ROS production is still operating? Indeed, when the IMD pathway is
437 disabled, bacteria are still confined in the anterior part of the gut, but are not effectively
438 eliminated, resulting in larval death. This outcome strongly suggests that ROS alone are
439 insufficient for bacterial eradication, even though they have been shown to damage and
440 inhibit bacterial proliferation (Benguettat et al., 2018; Ha et al., 2005). However, the role of
441 ROS in the immune response remains crucial since their timing of expression before
442 antimicrobial peptides is likely a key factor for the efficiency of the immune response. Our
443 findings, together with those from other studies, highlight the critical role of AMPs in fighting

444 off virulent intestinal bacteria, particularly in scenarios where ROS activity is compromised or
445 inadequate (Ramond et al., 2021; Ryu et al., 2006). Our findings emphasize the critical role of
446 the ROS/TrpA1/Dh31 axis in effectively eradicating ingested pathogens. The rapid production
447 of ROS following bacterial ingestion plays a pivotal role in closing the pylorus and retaining
448 virulent bacteria in the anterior midgut. Notably, this process does not necessitate a
449 transcriptional/translation response. In contrast, the production of antimicrobial peptides is a
450 lengthier process, involving the transcriptional activation of *AMP* genes downstream of the
451 IMD pathway, followed by their translation and secretion. The initial confinement of bacteria
452 in the anterior midgut allows time for AMPs to be produced to eliminate the trapped bacteria,
453 which is crucial for the organismal survival. This anterior lockdown is important since when
454 virulent bacteria reach the posterior midgut (in absence of ROS or in *TrpA1* or *Dh31* mutants)
455 the larvae die despite a functional IMD pathway. A key question arises: Is the posterior midgut
456 less equipped to combat bacteria? Research by (Bosco-Drayon et al., 2012) suggests that while
457 the posterior midgut can produce AMPs, this portion of the gut is predominantly dedicated to
458 the dampening the immune response, particularly through the production of amidases. This
459 permits an immune tolerance likely fostering the establishment of the commensal flora.
460 Consistent with this, we observed that commensal bacteria like *Lp* transit from the anterior to
461 the posterior midgut and persist there without compromising larval survival. Additionally, *Lp*
462 inherent resistance to AMPs (Arias-Rojas et al., 2023) further underscores the idea that the
463 anterior midgut serves as a checkpoint where certain bacteria are detained and eliminated,
464 while others, like *Lp*, are permitted to pass through. When the lockdown mechanism is
465 compromised, pathogens or pathobionts can spread into the posterior midgut, potentially
466 eliciting an inadequate dampened immune response. Thus, the anterior midgut acts as a
467 critical juncture in determining the fate of ingested bacteria, either leading to their elimination

468 or allowing their passage to the posterior midgut, where a more tolerant immune
469 environment prevails.

470 Understanding the practical application of this defense mechanism in the natural environment
471 of *Drosophila melanogaster* larvae is crucial. In the wild, *Drosophila* adults are typically drawn
472 to rotting fruits on which they lay eggs, exposing them and their progeny to a plethora of fungi
473 and bacteria. Consequently, developing larvae feed and grow in these non-sterile conditions.
474 In such environments, encountering pathogenic microbes is inevitable. Evasion or avoidance
475 behavior has been documented as a potential strategy for dealing with pathogens (Surendran
476 et al., 2017). This behavior might enable larvae to seek environments that will supposedly
477 better sustain their survival. However, given the larvae constant consumption of their
478 surrounding media in a race to reach pupation, ingestion of pathogen-contaminated food is a
479 common risk. Under these circumstances, larvae have limited options prior to the activation
480 of their innate immune response. Discriminating innocuous from potentially deleterious
481 bacteria and then locking down the latter ones for subsequent elimination by AMPs, clearly
482 benefits the host. Nonetheless, the effectiveness of this lockdown strategy would be
483 maximized if it were coordinated with evasion behaviors. Such coordination could prevent
484 repeated engagement in this energy-intensive immune response, thus optimizing the larvae
485 chances of reaching pupation successfully. This interplay between immune response and
486 behavioral adaptation underlines the sophisticated strategies employed by *Drosophila* larvae
487 to navigate their microbial-rich environment.

488

489 **MATERIALS AND METHODS**

490 **1-Bacterial strain**

491 We used the following strains: *Bacillus-thuringiensis*-GFP (*Bt*) (Hachfi et al., 2023) (the original
492 strain, 4D22, is from the Bacillus Genetics Stock Center - www.bgsc.org), *Erwinia carotovora*
493 subsp. *carotovora*-GFP *15* (*Ecc*) (Basset et al., 2000) and *Lactiplantibacillus plantarum*-GFP (*Lp*)
494 (gift from Renata Matos and François Leulier) (Storelli et al., 2018). *Bt* and *Ecc* were grown on
495 standard LB agar plates at 30°C and *Lp* was grown in MRS medium in anaerobic conditions at
496 37°C for at least 18 hours. Each bacterium was plated from glycerol stocks for each
497 experiment. A single colony was used to prepare liquid cultures. Bacteria were inoculated in
498 the 500 ml of appropriate medium. After overnight growth, the cultures were centrifuged for
499 15 min at 7500 rpm. Bacterial infectious doses were adjusted by measuring culture turbidity
500 at an optical density of 600 nm. OD_{600}=100 for *Lp* and *Ecc* corresponds to $4.9.10^7$CFU/µl.
501 OD_{600}=100 for *Bt* corresponds to $1,5.10^7$CFU/µl.

502 **2-FLY Stocks**

503 Flies were maintained at 25 °C on our standard fly medium (Nawrot-Esposito et al., 2020)
504 with12:12 light/dark cycle. Fly stocks used in this study and their origins are as follows: as a
505 reference in our experiments and noted as *ctrl*, we used Canton S (Bloomington #64349),
506 *TrpA1*^{1} (Bloomington #26504), *Dh31*^{KG09001} (Bloomington #16474), *Dh31-Gal4* (Bloomington
507 #51988), *PGRP-LC*$^{\Delta E}$ (Bloomington #55713), *PGRP-LE*^{112} (Bloomington #33055), *Dredd*^{F64} (Gift
508 from B. Charroux), *Relish*^{E20} (Bloomington #55714), *ΔAMP14* (Gift from B. Lemaitre; (Carboni
509 et al., 2022), *TrpA1*-Gal4/UAS-RFP (Gal4 is Bloomington #527593, UAS is Bloomington
510 #27392), *Da*-Gal4 (Bloomington #55851), *pros*-Gal4 (gift form B. Charroux), *Mex*-Gal4 (gift
511 from B. Charroux), UAS-*Duox _IR* (Bloomington #38907), UAS-*Dh31_IR*(Bloomington#25925).

512 **3-Infection experiments**

513 Oral infections were performed on mid-L3 larvae (3.5 days after egg laying). For each
514 experiment, between 20 and 50 non-wandering L3 larvae raised at 25°C were collected and
515 washed in PBS (1x). Bacterial pellets were mixed with yeast 40% in PBS (1x) and 500 µl of the
516 infected food were added at the bottom of an empty plastic fly vial (VWR) before adding the
517 larvae and sealing it with Parafilm. Then, the larvae were placed at 25°C in the dark. After
518 60min, the larvae were washed in PBS (1x) and then counted for the presence of GFP-bacteria
519 or for other analyses.

520 **4-Larvae dissection**

521 After 60 min, the infected larvae were washed in PBS (1x). Guts were dissected and fixed in
522 formaldehyde 4% for 45 min, then washed twice in PBS (1x) for 10 min. Guts were mounted
523 between poly-L-lysine (SIGMA P8920-100ML) coated slides and coverslips in Vectashield/DAPI
524 (Vector Laboratories).

525 **5- Colony-forming unit (CFU) counting**

526 Infected animals were washed in ethanol 70% for 30s then rinsed in PBS (1x). Guts were
527 dissected in PBS (1x) and homogenized with a micropestle in 200 µl of LB medium. Samples
528 were serially diluted in LB medium and plated on LB agar plates overnight at 30 °C. The
529 Colonies Forming Unit (CFU) were counted the following day. CFU counting has been
530 performed at 5 time points: 1h, 2h, 4h, 6h and 8h after a 60 min intoxication (at least 20 larvae
531 per point and 3 independent repeats).

532 **6-Mortality test**

533 Oral infection of the Larvae was performed as described above. Larvae of the different
534 genotypes fed 1h with *Bt*, *Lp* or *Ecc* were quickly washed in 70% ethanol and then PBS (1x).
535 Only the larvae that eaten (containing GFP bacteria in their intestine) were selected and put
536 in water for 18h at 25°C. Mortality was evaluated at this time-point.

537 **7- DTT and CGRP feeding**

538 Oral infection of the Larvae was performed as described above.
539 **DTT:** DTT was added to the food at a final concentration of 100 nM and larvae were fed during
540 60 min.
541 **hCGRP:** hCGRP (Sigma #C0167) was resuspended in distilled water. Larvae were fed 1h as
542 described above with a final hCGRP concentration of 400 µg/ml.

543 **8-Immunostaining**

544 Dissected intestines were washed twice with PBS (1x)-0.1% Triton X100 then incubated for 3h
545 in the blocking solution (10% of fetal calf serum, 0.1% Triton X100, PBS (1x)). The blocking
546 solution was removed and the primary antibodies added and incubated overnight à 4°C in
547 blocking solution. The following antibodies were used: mouse anti-Prospero (MR1A-c,
548 Developmental Studies Hybridoma Bank (DSHB)) at 1:200 and rabbit anti-Dh31 (gift from Jan
549 Veenstra and Michael Nitabach; (Kunst et al., 2014; Park et al., 2008) at 1:500. Secondary
550 antibodies used were anti-mouse Alexa647 (Invitrogen Cat# A-21235), anti-rabbit Alexa546
551 (Invitrogen Cat# A-11010). All secondary antibodies were used at 1:1000. Guts were mounted
552 in Fluoroshield-DAPI mounting medium (Sigma F6057). Observations of GFP producing
553 bacteria and of dTRPA1+ cells were done using the native fluorescence without
554 immunostaining.

555 **9-RNAi experiments**

556 All the tested animals were F1 obtained from a cross between parents possessing the Gal4
557 transgene and parents possessing the UAS-RNAi construction or from crosses between control
558 flies and transgenic animals. The larvae were then fed with contaminated food as described
559 above.

560 **10-Images and movie acquisition**

561 Images acquisition was performed at the microscopy platform of the Institut Sophia
562 Agrobiotech (INRAE 1355-UCA-CNRS 7254-Sophia Antipolis) with the macroscope Zeiss
563 AxioZoom V16 with an Apotome 2 or a Zeiss Axioplan Z1 with Apotome 2 microscope. Images
564 were analyzed using ZEN and Photoshop softwares. Movie acquisitions were performed with
565 the macroscope Zeiss AxioZoom V16 equipped with the Hamamatsu Flash 4LT Camera. Larvae
566 were captured every 5 minutes. Dead larva images were acquired with a numeric Keyence
567 VHX 2000 microscope.

568 **11-Data representation and statistical analyses**

569 The Graphpad Prism 8 software was used for statistical analyses.

570 CFU data analysis: the D'Agostino–Pearson test to assay whether the values are distributed
571 normally was applied. As not all the data sets were considered normal, non-parametric
572 statistical analysis such as non-parametric unpaired Mann–Whitney two-tailed tests was used
573 for all the data presented.

574 Lockdown ratio and survival ratio datasets: as the values obtained from one larva are
575 categorical data with a *Yes* or *No* value, we used the two-sided Fisher exact t-test and the 95%
576 confidence interval to test the statistical significance of a possible difference between a test
577 sample and the related control.

578 For all the quantitative assays, at least 3 independent experiments were performed and some
579 were done in two different laboratories by more than one experimenter. The results from all
580 the experiments were gathered and the total amount of larvae tested is indicated in the
581 source data file. In addition, we do not show the average response from one experiment
582 representative of the different biological replicates, but an average from all the data
583 generated during the independent experiments in one graph.

584 **12-Source data files: detailed lines, conditions and statistics for the figure section**

585 A file containing raw data, all the details about the experiments including the replicates,
586 sample size, genotypes and detailed statistical analyzes is available
587 (https://figshare.com/articles/dataset/Tleiss_et_al_lockdown_Source_Data_File/25018352
588 DOI:10.6084/m9.figshare.25018352).

589

590 **FIGURE LEGENDS**

591 **FIGURE 1**

592 **Contrary to *Lp*, *Ecc* or *Bt* bacteria are locked down in the anterior part of the gut.**

593 **A**: Pictures to illustrate the position of the green fluorescence of control L3 stage larvae as a
594 group (upper panel) or individual (lower panel) after having been fed 1h with a media
595 containing yeast and GFP-producing bacteria (*Ecc* or *Bt* or *Lp*). The white asterisk indicates the
596 anterior part of the animal. The white arrow indicates the posterior limit of the area containing
597 the fluorescent bacteria. Below the pictures are schematics representing larvae, their gut, and
598 the relative position of the GFP-producing bacteria in green. Scale bar is 1mm.

599 **B**: Graphic representing the lockdown ratio for L3 larvae exposed during 1h to a mixture
600 composed of yeast and fluorescent bacteria. The ratio of control larvae with a distinguishable
601 green fluorescence only in the upper part of the intestine, considered as locked-down
602 bacteria, is represented. The ratio is calculated as: x larvae with bacteria locked down/ (x
603 larvae with bacteria locked down + y larvae with bacteria all along the gut). Larvae with no
604 distinguishable fluorescence were considered as non-eaters and discarded from the
605 quantifications. The ratio of larvae with no distinguishable fluorescence was not influenced by
606 the different conditions we tested. Shown is the average lockdown ratio with a 95%
607 confidence interval from at least 3 independent assays with at least 30 animals per condition
608 and trial. **** indicates p<0,0001, Fischer exact t-test. See the source data file for details.

609

610

611 **FIGURE 2**

612 **Bacterial lockdown is dose-dependent, occurs in less than 30 minutes, and does not involve**
613 **a group effect.**

614 **A**: Lockdown ratio for control L3 larvae fed 1h with a mixture combining yeast with different
615 concentrations of fluorescent *Ecc* or *Bt*, concentrations are in number of bacteria per ml.
616 Shown is the average lockdown ratio with a 95% confidence interval from at least 3
617 independent assays with at least 18 animals per condition and trial. **** indicates p<0,0001,
618 Fischer exact t-test. See the source data file for details.

619 **B**: Representative images of control larvae fed during 30 min. with *Bt*. Scale bar is 1mm.

620 **C**: Lockdown ratio for control L3 larvae fed during various times with a mixture combining
621 yeast with *Ecc* or *Bt.* Shown is the average lockdown ratio with a 95% confidence interval from
622 at least 3 independent assays with at least 20 animals per condition and trial. ns indicates
623 values with differences not statistically significant, **** indicates p<0,0001, Fischer exact t-
624 test. See the source data file for details.

625 **D**: Lockdown ratio for control L3 larvae fed 1h as individual animals or as groups of 10 or >40
626 with a mixture combining yeast with a constant concentration of *Ecc* or *Bt* (4.10^{10} bacteria per
627 ml). Shown is the average lockdown ratio with a 95% confidence interval from at least 3
628 independent assays with the exact number of animals indicated per condition and trial. ns
629 indicates values with differences not statistically significant, Fischer exact t-test. See the
630 source data file for details.

631

632

633 **FIGURE 3**

634 **The bacterial lockdown necessitates Duox in enterocytes, the TrpA1 nociceptor and Dh31 in**
635 **enteroendocrine cells.**

636 **A**: Pictures to illustrate the localization of the fluorescent bacteria within the intestine of
637 control (ctrl), *Trpa1*[1] or *Dh31*$^{-}$ L3 larvae after having been fed 1h with a mixture of yeast and
638 *Ecc*. Scale bar is 1mm.

639 **B**: Lockdown ratio for control (ctrl) L3 larvae or mutants for *Trpa1*[1] or *Dh31*$^{-}$ fed 1h with a
640 mixture combining yeast and *Lp* or *Ecc* or *Bt* or fluorescent Dextran with or without hCGRP
641 hormone. Shown is the average lockdown ratio with a 95% confidence interval from at least 3
642 independent assays with at least 30 animals per condition and trial. 0 indicates an absence of
643 lockdown. **** indicates p<0,0001, Fischer exact t-test. See the source data file for details.

644 **C**: Pictures to illustrate the localization of the fluorescence within the intestine of control L3
645 larvae after having been fed 1h with a mixture of yeast and fluorescent Dextran with or
646 without hCGRP hormone. Below the pictures are schematics representing larvae, their gut,
647 and the relative position of the fluorescence in green. Scale bar is 1mm.

648 **D**: Lockdown ratio for animals expressing RNA interference constructions directed against
649 *Duox* mRNA or *Dh31* mRNA, ubiquitously (Da-Gal4), in enterocytes (Mex-Gal4) or in
650 enteroendocrine cells (Pros-Gal4) and then fed 1h with a mixture combining yeast and *Ecc* or
651 *Bt*. Shown is the average lockdown ratio with a 95% confidence interval from at least 3
652 independent assays with at least 30 animals per condition and trial. ns indicates values with
653 differences not statistically significant, **** indicates p<0,0001 , Fischer exact t-test. See the
654 source data file for details.

655 **FIGURE 4**

656 **Blocking the ROS with DTT prevents the lockdown of *Bt* and the larvae with bacteria in the**
657 **posterior part of the intestine die.**

658 **A**: Pictures to illustrate the localization of the fluorescence within the intestine of control
659 (ctrl) L3 larvae after having been fed 1h with a mixture of yeast and *Bt* with or without DTT.
660 Below the pictures are schematics representing larvae, their gut, and the relative position of
661 the fluorescent bacteria in green. Scale bar is 1mm.

662 **B**: Lockdown ratio for control (ctrl) L3 larvae fed 1h with a mixture combining yeast, DTT and
663 fluorescent Dextran or *Bt*. Shown is the average lockdown ratio with a 95% confidence interval
664 from at least 3 independent assays with at least 18 animals per condition and trial. ns indicates
665 values with differences not statistically significant, Fischer exact t-test. See the source data file
666 for details.

667

668 **FIGURE 5**

669 **In the absence of lockdown in *TrpA1*[1] or *Dh31*⁻ mutants, *Bt* and *Ecc* proliferate in the larval**
670 **intestine and the larvae die.**

671 **A**, **B** and **C**: quantification over time of the amount of *Lp*, (A), *Bt* (B) or *Ecc* (C) live bacteria
672 within the larval intestine of control (ctrl) (A, B and C), *Dh31*⁻ (B and C) and *TrpA1*[1] (B and C)
673 animals following a 1h feeding period with a solution containing yeast and bacteria. CFU
674 stands for Colony Forming Units. Shown is the average ± SEM of at least 3 independent
675 experiments with at least 7 guts each. After 8h, either all the *TrpA1*[1] or *Dh31*⁻ larvae were
676 dead or the intestines were severely damaged preventing the CFU counting. * Indicates
677 p<0,05, Mann Whitney, two-tailed test. See the source data file for details.

678 **D**: Pictures of control (ctrl) or *TrpA1*[1] or *Dh31*⁻ larvae after 8h in water following a 1h feeding
679 with a mixture of yeast and *Bt.* For control larvae, some animals made pupae that are visible
680 while for *TrpA1*[1] and *Dh31*⁻mutants, the dark larvae are dead non-moving melanized animals.
681 Scale bar is 1mm.

682 **E**: Ratio of dead control or T*rpA1*[1] or *Dh31*⁻ larvae after 8h in water following or not (water)
683 a 1h feeding period with yeast mixed with *Lp* or *Ecc* or *Bt.* Shown is the average with 95%
684 confidence interval of at least 3 independent experiments with at least 21 larvae per trial and
685 condition. The 0 symbol indicates an absence of lethality. **** indicates p<0,0001, Fischer
686 exact t-test. See the source data file for details.

687 **F**: Ratio of dead control (ctrl) larvae after 8h in water following a 1h feeding period with a
688 mixture combining yeast, DTT and Dextran fluorescent beads or *Bt*. Shown is the average with
689 95% confidence interval of at least 3 independent experiments with at least 18 larvae per trial

690 and condition. The 0 symbol indicates an absence of lethality. **** indicates p<0,0001, Fischer

691 exact t-test. See the source data file for details.

692 **FIGURE 6**

693 **TrpA1+ cells are enteroendocrine cells concentrated in a portion of the intestine bordering**
694 **the locked-down bacteria.**

695 Confocal fluorescent pictures of the anterior portions of L3 larval intestines to detect;
696 longitudinal and transversal muscles concentrated in actin (F, G, H and H'), TrpA1+ cells
697 producing RFP (A, A', B, C, C'' and F), GFP-bacteria (B, G and H), Dh31+ cells (C', C'', D and E),
698 Pros+ cells (D and E) and nuclei with DNA staining (A, A', B, C'', D, E and G).

699 In B, D, E, G, H and H'; animals were previously fed for 1h with a mixture containing bacteria
700 and yeast with *Bt* (B, D and E) or *Ecc* (G, H and H'). When present, the white star indicates the
701 anterior part of the intestinal portion shown, the arrows point to TARMs and the > symbols
702 point to TrpA1+ cells. The empty squares in A and H with dashed lines correspond to the
703 portion of the image magnified in A' and H', respectively. Scale bar in A, B, F, G and H
704 represents 500µm, in A', C, D, E and H' represents 100 µm.

705

706 **FIGURE 7**

707 **IMD pathway is not required for the lockdown but essential for larvae survival and *Bt* or *Ecc***
708 **clearance**

709 **A**: Pictures to illustrate the localization of the fluorescence within the intestine of *PGRP-*
710 *LC*$^{[\Delta E]}$ L3 larvae after having been fed 1h with a mixture of *Lp* or *Ecc* or *Bt*. Scale bar is 1mm.

711 **B**: Lockdown ratio for control L3 larvae or mutants of the IMD pathway fed 1h with a mixture
712 combining yeast and *Lp* or *Ecc* or *Bt*. Shown is the average with 95% confidence interval of at
713 least 3 independent experiments with at least 20 larvae per trial and condition. ns indicates
714 values with differences not statistically significant, Fischer exact t-test. See the source data file
715 for details.

716 **C**: Pictures of *PGRP-LC*$^{[\Delta E]}$, *Rel*$^{[E20]}$ or *ΔAMP14* mutant larvae after 18h in water following a 1h
717 feeding with a mixture of yeast and *Bt*. The dark larvae are dead non-moving melanized
718 animals. *ΔAMP14* is a mutant deleted for 14 antimicrobial-encoding genes.

719 **D**: Ratio of dead control or *TrpA1*$^{[1]}$ or *Dh31*$^{-}$ larvae after 18h in water following or not (water)
720 a 1h feeding period with yeast mixed with *Lp* or *Ecc* or *Bt.* Shown is the average with 95%
721 confidence interval of at least 3 independent experiments with at least 20 larvae per trial and
722 condition. The 0 symbol indicates an absence of lethality. **** indicates p<0,0001, Fischer
723 exact t-test. See the source data file for details.

724 **E** and **F**: quantification over time of the amount of *Bt* (A) and *Ecc* (B) live bacteria within the
725 larval intestine of control or IMD pathway mutant animals including *ΔAMP14* following a 1h
726 feeding period with a solution containing yeast and bacteria. CFU stands for Colony Forming
727 Units. *ΔAMP14* is a mutant deleted for 14 antimicrobial-encoding genes. Shown is the average

728 ± SEM of at least 3 independent experiments with at least 7 guts each. After 8h, either all the

729 mutants were dead or the intestines were severely damaged preventing the CFU counting. *

730 Indicates p<0,05, Mann Whitney, two-tailed test. See the source data file for details.

731

732

733 **FIGURE 8**

734 **Chronological coordination of ROS/TrpA1/Dh31 and IMD pathways for an efficient microbial**
735 **elimination**

736 **t0:** larvae ingest bacteria from the food mixture (anterior on the left, only bacteria similar to
737 *Ecc* or *Bt* are illustrated). This initial phase necessitates a discrimination between commensal
738 and pathogenic bacteria, not elucidated in this study (symbolized by '?'). The presence of
739 pathogenic bacteria induces the production of ROS by enterocytes (EC) in a Duox-dependent
740 manner. Then ROS activates TrpA1 in enteroendocrine cells (EEC). **t15 minutes:** Dh31
741 secretion by EEC is responsible for the lockdown of bacteria likely by promoting visceral
742 muscle contractions leading to a closure of a pylorus-like structure. This phenomenon
743 concentrates the bacteria in the anterior part of the gut. The bacterial concentration in this
744 part of the intestinal lumen may facilitate the triggering of the IMD signaling cascade that
745 controls the transcription of the genes (*AMPs*) encoding the antimicrobial peptides (AMPs). **t6**
746 **hours:** the pylorus-like structure is still closed. The bactericidal activity of AMPs has eliminated
747 most of the bacteria accumulated in the anterior part of the intestine. Importantly, if
748 confinement is prevented, the larvae die; if the response by antimicrobial peptides is
749 hindered, the larvae die.

750

751

752 **SUPP1**

753 ***Ecc* and *Bt* are locked down in the anterior part of the intestine and disappear while *Lp***

754 **transits to the posterior part and remains.**

755 **A**: Timelapse from the movies of L3 Larvae fed 1h with a mixture of yeast and *Ecc* then

756 transferred on a glass slide to be imaged overnight. Refers to Movie 1.

757 **B**: Timelapse from the movies of L3 Larvae fed 1h with a mixture of yeast and *Bt* then

758 transferred on a glass slide to be imaged overnight. Refers to Movie 2.

759 **C**: Timelapse from the movies of L3 Larvae fed 1h with a mixture of yeast and *Lp* then

760 transferred on a glass slide to be imaged overnight. Refers to Movie 3.

761 For A-C, the frames are separated by 5 minutes.

762 **SUPP2**

763 **Contrary to *Lp*, *Ecc* or *Bt* bacteria are locked down in the anterior part of the gut.**

764 **A**: Graphic representing the lockdown ratio for dissected intestines of L3 larvae exposed
765 during 1h to a mixture composed of yeast and fluorescent bacteria. Shown is the average
766 lockdown ratio with a 95% confidence interval from at least 3 independent assays with at least
767 8 organs per condition and trial. **** indicates p<0,0001, Fischer exact t-test. See the source
768 data file for details.

769

770 **SUPP3**

771 ***Ecc* is not locked down anteriorly in *TrpA1*$^{[1]}$ and *Dh31*$^{-}$ mutants, persists in the posterior**
772 **part of the intestine and disappear while *Lp* can be locked down following exogenous**
773 **addition of hCGRP.**

774 **A**: Timelapse from the movies of *TrpA1*$^{[1]}$ L3 Larvae fed 1h with a mixture of yeast and *Ecc*
775 then transferred on a glass slide to be imaged overnight. Refers to Movie 4.

776 **B**: Timelapse from the movies of *Dh31*$^{-}$ L3 Larvae fed 1h with a mixture of yeast and *Ecc* then
777 transferred on a glass slide to be imaged overnight. Refers to Movie 5.

778 **C**: Timelapse from the movies of w^{-} L3 Larvae fed 1h with a mixture of yeast and *Lp* + hCGRP
779 then transferred on a glass slide to be imaged overnight. Refers to Movie 6.

780 For A-C, the frames are separated by 5 minutes.

781

782 **SUPP4**

783 Confocal fluorescent pictures of different TARMsT2 in the anterior portions of L3 larval
784 intestines to detect longitudinal and transversal muscles concentrated in actin The white star
785 indicates the anterior part of the intestinal portion shown. The empty square with dashed
786 lines in A corresponds to the portion of the image magnified in A'. Scale bar represents 500µm.

787

SUPP5

***Bt* and *Ecc* are locked down anteriorly and persist in *PGRP-LC*$^{[\Delta E]}$ *and PGRP-LE*$^{[112]}$ mutants, respectively.**

A: Timelapse from the movies of *PGRP-LC*$^{[\Delta E]}$ L3 Larvae fed 1h with a mixture of yeast and *Bt* then transferred on a glass slide to be imaged overnight. Refers to Movie 8.

B: Timelapse from the movies of *PGRP-LE*$^{[112]}$ L3 Larvae fed 1h with a mixture of yeast and *Ecc* then transferred on a glass slide to be imaged overnight. Refers to Movie 9.

For A and B, the frames are separated by 5 minutes.

SUPP6

***Bt* and *Ecc* are locked down and persist anteriorly in *Dredd*$^{[F64]}$ *and Rel*$^{[E20]}$ mutants.**

A: Timelapse from the movies of *Dredd*$^{[F64]}$ L3 Larvae fed 1h with a mixture of yeast and *Ecc* then transferred on a glass slide to be imaged overnight. Refers to Movie 10.

B: Timelapse from the movies of *Rel*$^{[E20]}$ L3 Larvae fed 1h with a mixture of yeast and *Bt* then transferred on a glass slide to be imaged overnight. Refers to Movie 11.

C: Timelapse from the movies of *Rel*$^{[E20]}$ L3 Larvae fed 1h with a mixture of yeast and *Ecc* then transferred on a glass slide to be imaged overnight. Refers to Movie 12.

For A-C, the frames are separated by 5 minutes.

808 **MOVIES**

809 **Movie 1**

810 https://figshare.com/articles/media/ctrl_vs_Ecc-gfp/25018385

811 **DOI: 10.6084/m9.figshare.25018385**

812 **Fluorescent *Ecc* is locked down in the anterior part of the larval intestine then vanishes.**

813 Live imaging during 12h of a L3 control larva previously fed 1h with a food containing *Ecc*

814 fluorescent bacteria then transferred on a glass slide in a wet chamber.

815

816 **Movie 2**

817 https://figshare.com/articles/media/2-ctrl_vs_Bt-GFP/25018427

818 **DOI: 10.6084/m9.figshare.25018427**

819 **Fluorescent *Bt* is locked down in the anterior part of the larval intestine then vanishes.**

820 Live imaging during 12h of a L3 control larva previously fed 1h with a food containing *Bt*

821 fluorescent bacteria then transferred on a glass slide in a wet chamber.

822

823 **Movie 3**

824 https://figshare.com/articles/media/Tleiss_et_al_Movie_3-ctrl_vs_Lp_avi/25018442

825 **DOI: 10.6084/m9.figshare.25018442**

826 **Fluorescent *Lp* is not locked down in the anterior part of the larval intestine and persists in**

827 **the posterior midgut.**

828 Live imaging during 10h of a L3 control larva previously fed 1h with a food containing *Lp*
829 fluorescent bacteria then transferred on a glass slide in a wet chamber.

830

831 **Movie 4**

832 https://figshare.com/articles/media/Tleiss_et_al_Movie_4_TrpA1_vs_Ecc-gfp/25018463

833 **DOI :10.6084/m9.figshare.25018463**

834 **Fluorescent *Ecc* is not locked down in the anterior part of the *TrpA1* mutant larval intestine**
835 **and persists in the posterior midgut.**

836 Live imaging during 10h of a L3 *TrpA1* mutant larva previously fed 1h with a food containing
837 *Ecc* fluorescent bacteria then transferred on a glass slide in a wet chamber.

838

839 **Movie 5**

840 https://figshare.com/articles/media/Tleiss_et_al_Movie_5_Dh31_vs_Ecc/25018472

841 **DOI: 10.6084/m9.figshare.25018472**

842 **Fluorescent *Ecc* is not locked down in the anterior part of the *Dh31* mutant larval intestine**
843 **and persists in the posterior midgut.**

844 Live imaging during 10h of a L3 *Dh31* mutant larva previously fed 1h with a food containing
845 *Ecc* fluorescent bacteria then transferred on a glass slide in a wet chamber.

846

847

848 **Movie 6**

849 https://figshare.com/articles/media/Tleiss_et_al_Movie_6_ctrl_vs_Lp_vs_hCGRP/250184

850 81

851 **DOI: 10.6084/m9.figshare.25018481**

852 **Fluorescent *Lp* is locked down in the anterior part of the larval intestine following treatment**

853 **with hCGRP.**

854 Live imaging during 12h of a control L3 larva previously fed 1h with a food containing *Lp*

855 fluorescent bacteria and hCGRP then transferred on a glass slide in a wet chamber.

856

857 **Movie 7**

858 https://figshare.com/articles/media/Tleiss_et_al_Movie_7_TARM_T2_3D/25018496

859 **DOI: 10.6084/m9.figshare.25018496**

860 **TARMsT2 are attached to the longitudinal gut muscles.**

861 Confocal imaging of the intestine from a control animal stained with fluorescent phalloidin

862 and animated 3D-reconstruction of the anterior portion containing the attached TARMs.

863

864 **Movie 8**

865 https://figshare.com/articles/media/Tleiss_et_al_Movie_8_pgrp-lc_vs_Bt/25018499

866 **DOI :10.6084/m9.figshare.25018499**

867 **Fluorescent *Bt* is locked down in the anterior part of the *PGRP-LC* mutant larval intestine**
868 **and persists.**

869 Live imaging during 12h of a L3 *PGRP-LC* mutant larva previously fed 1h with a food containing
870 *Bt* fluorescent bacteria then transferred on a glass slide in a wet chamber.

871

872 **Movie 9**

873 https://figshare.com/articles/media/Tleiss_et_al_Movie_9_pgrp-le_vs_Ecc/25018505

874 **DOI: 10.6084/m9.figshare.25018505**

875 **Fluorescent *Ecc* is locked down in the anterior part of the *PGRP-LE* mutant larval intestine**
876 **and persists.**

877 Live imaging during 12h of a L3 *PGRP-LE* mutant larva previously fed 1h with a food containing
878 *Ecc* fluorescent bacteria then transferred on a glass slide in a wet chamber.

879

880 **Movie 10**

881 https://figshare.com/articles/media/Tleiss_et_al_Movie_10_Dredd_vs_Ecc/25018517

882 **DOI: 10.6084/m9.figshare.25018517**

883 **Fluorescent *Ecc* is locked down in the anterior part of the *Dredd* mutant larval intestine and**
884 **persists.**

885 Live imaging during 12h of a L3 *Dredd* mutant larva previously fed 1h with a food containing
886 *Ecc* fluorescent bacteria then transferred on a glass slide in a wet chamber.

887

888 **Movie 11**

889 https://figshare.com/articles/media/Tleiss_et_al_Movie_11_Rel_vs_Bt/25018529

890 **DOI: 10.6084/m9.figshare.25018529**

891 **Fluorescent *Bt* is locked down in the anterior part of the *Rel* mutant larval intestine and**

892 **persists.**

893 Live imaging during 12h of a L3 *Rel* mutant larva previously fed 1h with a food containing *Bt*

894 fluorescent bacteria then transferred on a glass slide in a wet chamber.

895

896 **Movie 12**

897 https://figshare.com/articles/media/tleiss_et_al_Movie_12_Rel_vs_Ecc/25018538

898 **DOI: 10.6084/m9.figshare.25018538**

899 **Fluorescent *Ecc* is locked down in the anterior part of the *Rel* mutant larval intestine and**

900 **persists.**

901 Live imaging during 12h of a L3 *Rel* mutant larva previously fed 1h with a food containing *Ecc*

902 fluorescent bacteria then transferred on a glass slide in a wet chamber.

903

904

905

906 **AUTHOR CONTRIBUTIONS**

907 L.K., A.G., F.T., M.M., O.P., D.O. and J.R. conceived the experiments. F.T., M.M., O.P.
908 performed the experiments. L.K., A.G., F.T., D.O. and J.R. wrote the manuscript. A.G., D.O. and
909 J.R. secured funding.

910 **COMPETING INTERESTS**

911 The authors have declared that no competing interests exist.

912 **ACKNOWLEDGMENTS**

913 We are grateful to all members of the BES and DEB teams at the Institut Sophia Agrobiotech
914 for fruitful discussions. We greatly thank Emilie Avazéri, Gladys Gazelle, Marie-Paule Esposito,
915 Juliette Dubois and Elisa Di Lelio for their technical support. We thank Bernard Charroux (at
916 the IBDM Aix Marseille University) and Ambra MASUZZO (in the team of Richard Benton,
917 Université de Lausanne) for pioneer observations and numerous discussions, François Leulier
918 and Renata Matos for sharing bacterial and fly lines and Frank Schnorrer for discussions about
919 alary muscles.

920 **FUNDING**

921 F.T. was supported by the Lebanese Association for Scientific Research (LASER), the AJAJE
922 association from Lebanon, and the Université Côte d'Azur (ATER). This work was supported by
923 the French government through the UCAJEDI Investments in the Future project managed by
924 the National Research Agency (ANR) with the reference number ANR-15-IDEX-01 and through
925 the ANR-22-CE35-0006-01 (BaDAss) to A.G. This work was supported by CNRS, ANR
926 BACNEURODRO (ANR-17-CE16-0023-01), Equipe Fondation pour la Recherche Médicale
927 (EQU201603007783) and the ANR Pepneuron (ANR-21-CE16-0027) to J.R. and L.K.

928 **REFERENCES**

929 **Arias-Rojas, A., Frahm, D., Hurwitz, R., Brinkmann, V. and Iatsenko, I.** (2023). Resistance to host
930 antimicrobial peptides mediates resilience of gut commensals during infection and aging in Drosophila.
931 *Proc Natl Acad Sci U S A* **120**, e2305649120.
932 **Basset, A., Khush, R. S., Braun, A., Gardan, L., Boccard, F., Hoffmann, J. A. and Lemaitre, B.** (2000).
933 The phytopathogenic bacteria Erwinia carotovora infects Drosophila and activates an immune
934 response. *Proc Natl Acad Sci U S A* **97**, 3376-81.
935 **Bataillé, L., Colombié, N., Pelletier, A., Paululat, A., Lebreton, G., Carrier, Y., Frendo, J. L. and Vincent,**
936 **A.** (2020). Alary muscles and thoracic alary-related muscles are atypical striated muscles involved in
937 maintaining the position of internal organs. *Development* **147**.
938 **Belinskaia, M., Wang, J., Kaza, S. K., Antoniazzi, C., Zurawski, T., Dolly, J. O. and Lawrence, G. W.**
939 (2023). Bipartite Activation of Sensory Neurons by a TRPA1 Agonist Allyl Isothiocyanate Is Reflected by
940 Complex Ca(2+) Influx and CGRP Release Patterns: Enhancement by NGF and Inhibition with VAMP and
941 SNAP-25 Cleaving Botulinum Neurotoxins. *Int J Mol Sci* **24**.
942 **Benguettat, O., Jneid, R., Soltys, J., Loudhaief, R., Brun-Barale, A., Osman, D. and Gallet, A.** (2018).
943 The DH31/CGRP enteroendocrine peptide triggers intestinal contractions favoring the elimination of
944 opportunistic bacteria. *PLoS Pathog.* **14**, e1007279. doi: 10.1371/journal.ppat.1007279. eCollection
945 2018 Sep.
946 **Bosco-Drayon, V., Poidevin, M., Boneca, I. G., Narbonne-Reveau, K., Royet, J. and Charroux, B.**
947 (2012). Peptidoglycan sensing by the receptor PGRP-LE in the Drosophila gut induces immune
948 responses to infectious bacteria and tolerance to microbiota. *Cell Host Microbe* **12**, 153-65.
949 **Bulc, M., Palus, K., Całka, J. and Zielonka, Ł.** (2018). Changes in Immunoreactivity of Sensory
950 Substances within the Enteric Nervous System of the Porcine Stomach during Experimentally Induced
951 Diabetes. *J Diabetes Res* **2018**, 4735659.
952 **Capo, F., Charroux, B. and Royet, J.** (2016). Bacteria sensing mechanisms in Drosophila gut: Local and
953 systemic consequences. *Dev Comp Immunol* **64:11-21.**, 10.1016/j.dci.2016.01.001. Epub 2016 Jan 8.
954 **Carboni, A. L., Hanson, M. A., Lindsay, S. A., Wasserman, S. A. and Lemaitre, B.** (2022). Cecropins
955 contribute to Drosophila host defense against a subset of fungal and Gram-negative bacterial infection.
956 *Genetics* **220**.
957 **Chakrabarti, S., Liehl, P., Buchon, N. and Lemaitre, B.** (2012). Infection-induced host translational
958 blockage inhibits immune responses and epithelial renewal in the Drosophila gut. *Cell Host Microbe*
959 **12**, 60-70. doi: 10.1016/j.chom.2012.06.001.
960 **Chen, J., Kim, S. M. and Kwon, J. Y.** (2016). A Systematic Analysis of Drosophila Regulatory Peptide
961 Expression in Enteroendocrine Cells. 10.14348/molcells.2016.0014.
962 **Dombrovski, M., Kim, A., Poussard, L., Vaccari, A., Acton, S., Spillman, E., Condron, B. and Yuan, Q.**
963 (2019). A Plastic Visual Pathway Regulates Cooperative Behavior in Drosophila Larvae. *Curr Biol* **29**,
964 1866-1876.e5.
965 **Dombrovski, M., Poussard, L., Moalem, K., Kmecova, L., Hogan, N., Schott, E., Vaccari, A., Acton, S.**
966 **and Condron, B.** (2017). Cooperative Behavior Emerges among Drosophila Larvae. *Curr Biol* **27**, 2821-
967 2826.e2.
968 **Du, E. J., Ahn, T. J., Kwon, I., Lee, J. H., Park, J. H., Park, S. H., Kang, T. M., Cho, H., Kim, T. J., Kim, H.**
969 **W. et al.** (2016a). TrpA1 Regulates Defecation of Food-Borne Pathogens under the Control of the Duox
970 Pathway. *PLoS Genet* **12**, e1005773. doi: 10.1371/journal.pgen.1005773. eCollection 2016 Jan.
971 **Du, E. J., Ahn, T. J., Wen, X., Seo, D. W., Na, D. L., Kwon, J. Y., Choi, M., Kim, H. W., Cho, H. and Kang,**
972 **K.** (2016b). Nucleophile sensitivity of Drosophila TRPA1 underlies light-induced feeding deterrence.
973 *Elife* **5**.
974 **Earl, S. C., Rogers, M. T., Keen, J., Bland, D. M., Houppert, A. S., Miller, C., Temple, I., Anderson, D.**
975 **M. and Marketon, M. M.** (2015). Resistance to Innate Immunity Contributes to Colonization of the
976 Insect Gut by Yersinia pestis. *PLoS One* **10**, e0133318.

977 **Gu, P., Gong, J., Shang, Y., Wang, F., Ruppell, K. T., Ma, Z., Sheehan, A. E., Freeman, M. R. and Xiang,**
978 **Y.** (2019). Polymodal Nociception in Drosophila Requires Alternative Splicing of TrpA1. *Curr Biol* **29**,
979 3961-3973.e6.
980 **Guntur, A. R., Gu, P., Takle, K., Chen, J., Xiang, Y. and Yang, C. H.** (2015). Drosophila TRPA1 isoforms
981 detect UV light via photochemical production of H2O2. *Proc Natl Acad Sci U S A* **112**, E5753-61.
982 **Guo, X., Lv, J. and Xi, R.** (2021). The specification and function of enteroendocrine cells in Drosophila
983 and mammals: a comparative review. *Febs j*.
984 **Ha, E. M., Lee, K. A., Seo, Y. Y., Kim, S. H., Lim, J. H., Oh, B. H., Kim, J. and Lee, W. J.** (2009).
985 Coordination of multiple dual oxidase-regulatory pathways in responses to commensal and infectious
986 microbes in drosophila gut. *Nat Immunol* **10**, 949-57. doi: 10.1038/ni.1765. Epub 2009 Aug 9.
987 **Ha, E. M., Oh, C. T., Bae, Y. S. and Lee, W. J.** (2005). A direct role for dual oxidase in Drosophila gut
988 immunity. *Science* **310**, 847-50.
989 **Hachfi, S., Brun-Barale, A., Munro, P., Nawrot-Esposito, M.-P., Michel, G., Fichant, A., Bonis, M.,**
990 **Ruimy, R., Boyer, L. and Gallet, A.** (2023). Ingestion of Bacillus cereus spores dampens the immune
991 response to favor bacterial persistence. *bioRxiv*.
992 **Hanson, M. A. and Lemaitre, B.** (2020). New insights on Drosophila antimicrobial peptide function in
993 host defense and beyond. *Curr Opin Immunol* **62**, 22-30.
994 **Hegedus, D., Erlandson, M., Gillott, C. and Toprak, U.** (2009). New insights into peritrophic matrix
995 synthesis, architecture, and function. *Annu Rev Entomol* **54**, 285-302.
996 **Kaneko, T., Yano, T., Aggarwal, K., Lim, J. H., Ueda, K., Oshima, Y., Peach, C., Erturk-Hasdemir, D.,**
997 **Goldman, W. E., Oh, B. H. et al.** (2006). PGRP-LC and PGRP-LE have essential yet distinct functions in
998 the drosophila immune response to monomeric DAP-type peptidoglycan. *Nat Immunol* **7**, 715-23.
999 **Kasacka, I.** (2009). Quantitative distribution and localization of calcitonin gene-related peptide-like
1000 cells in the stomach of two kidney, one clip rats. *J Physiol Pharmacol* **60**, 35-9.
1001 **Keita, S., Masuzzo, A., Royet, J. and Kurz, C. L.** (2017). Drosophila larvae food intake cessation
1002 following exposure to Erwinia contaminated media requires odor perception, Trpa1 channel and evf
1003 virulence factor. *J Insect Physiol.* **99:25-32.**, 10.1016/j.jinsphys.2017.02.004. Epub 2017 Feb 21.
1004 **Kondo, T., Oshima, T., Obata, K., Sakurai, J., Knowles, C. H., Matsumoto, T., Noguchi, K. and Miwa,**
1005 **H.** (2010). Role of transient receptor potential A1 in gastric nociception. *Digestion* **82**, 150-5.
1006 **Kunst, M., Hughes, M. E., Raccuglia, D., Felix, M., Li, M., Barnett, G., Duah, J. and Nitabach, M. N.**
1007 (2014). Calcitonin gene-related peptide neurons mediate sleep-specific circadian output in Drosophila.
1008 *Curr Biol* **24**, 2652-64.
1009 **LaJeunesse, D. R., Johnson, B., Presnell, J. S., Catignas, K. K. and Zapotoczny, G.** (2010). Peristalsis in
1010 the junction region of the Drosophila larval midgut is modulated by DH31 expressing enteroendocrine
1011 cells. *BMC Physiol* **10:14.**, 10.1186/1472-6793-10-14.
1012 **Lapointe, T. K. and Altier, C.** (2011). The role of TRPA1 in visceral inflammation and pain. *Channels* **5**,
1013 525-9. doi: 10.4161/chan.5.6.18016. Epub 2011 Nov 1.
1014 **Lee, K. A., Kim, S. H., Kim, E. K., Ha, E. M., You, H., Kim, B., Kim, M. J., Kwon, Y., Ryu, J. H. and Lee,**
1015 **W. J.** (2013). Bacterial-derived uracil as a modulator of mucosal immunity and gut-microbe
1016 homeostasis in Drosophila. *Cell* **153**, 797-811. doi: 10.1016/j.cell.2013.04.009.
1017 **Lemaitre, B. and Miguel-Aliaga, I.** (2013). The digestive tract of Drosophila melanogaster. *Annu Rev*
1018 *Genet* **47:377-404.**, 10.1146/annurev-genet-111212-133343.
1019 **Leulier, F., Parquet, C., Pili-Floury, S., Ryu, J. H., Caroff, M., Lee, W. J., Mengin-Lecreulx, D. and**
1020 **Lemaitre, B.** (2003). The Drosophila immune system detects bacteria through specific peptidoglycan
1021 recognition. *Nat Immunol* **4**, 478-84.
1022 **Liehl, P., Blight, M., Vodovar, N., Boccard, F. and Lemaitre, B.** (2006). Prevalence of local immune
1023 response against oral infection in a Drosophila/Pseudomonas infection model. *PLoS Pathog.* **2**, e56.
1024 doi: 10.1371/journal.ppat.0020056. Epub 2006 Jun 9.
1025 **Loudhaief, R., Brun-Barale, A., Benguettat, O., Nawrot-Esposito, M. P., Pauron, D., Amichot, M. and**
1026 **Gallet, A.** (2017). Apoptosis restores cellular density by eliminating a physiologically or genetically
1027 induced excess of enterocytes in the Drosophila midgut. *Development* **144**, 808-819. doi:
1028 10.1242/dev.142539.

1029 **Louis, M. and de Polavieja, G.** (2017). Collective Behavior: Social Digging in Drosophila Larvae. *Curr*
1030 *Biol* **27**, R1010-r1012.
1031 **Mast, J. D., De Moraes, C. M., Alborn, H. T., Lavis, L. D. and Stern, D. L.** (2014). Evolved differences in
1032 larval social behavior mediated by novel pheromones. *Elife* **3**, e04205.
1033 **Nässel, D. R. and Zandawala, M.** (2019). Recent advances in neuropeptide signaling in Drosophila,
1034 from genes to physiology and behavior. *Prog Neurobiol* **179**, 101607.
1035 **Nawrot-Esposito, M. P., Babin, A., Pasco, M., Poirié, M., Gatti, J. L. and Gallet, A.** (2020). Bacillus
1036 thuringiensis Bioinsecticides Induce Developmental Defects in Non-Target Drosophila melanogaster
1037 Larvae. *Insects* **11**.
1038 **Neyen, C., Bretscher, A. J., Binggeli, O. and Lemaitre, B.** (2014). Methods to study Drosophila
1039 immunity. *Methods* **68**, 116-28. doi: 10.1016/j.ymeth.2014.02.023. Epub 2014 Mar 12.
1040 **Ogawa, N., Kurokawa, T. and Mori, Y.** (2016). Sensing of redox status by TRP channels. *Cell Calcium*
1041 **60**, 115-22. doi: 10.1016/j.ceca.2016.02.009. Epub 2016 Mar 4.
1042 **Park, D., Veenstra, J. A., Park, J. H. and Taghert, P. H.** (2008). Mapping peptidergic cells in Drosophila:
1043 where DIMM fits in. *PLoS One.* **3**, e1896. doi: 10.1371/journal.pone.0001896.
1044 **Pelaseyed, T., Bergstrom, J. H., Gustafsson, J. K., Ermund, A., Birchenough, G. M., Schutte, A., van**
1045 **der Post, S., Svensson, F., Rodriguez-Pineiro, A. M., Nystrom, E. E. et al.** (2014). The mucus and mucins
1046 of the goblet cells and enterocytes provide the first defense line of the gastrointestinal tract and
1047 interact with the immune system. *Immunol Rev* **260**, 8-20. doi: 10.1111/imr.12182.
1048 **Ramond, E., Jamet, A., Ding, X., Euphrasie, D., Bouvier, C., Lallemant, L., He, X., Arbibe, L., Coureuil,**
1049 **M. and Charbit, A.** (2021). Reactive Oxygen Species-Dependent Innate Immune Mechanisms Control
1050 Methicillin-Resistant Staphylococcus aureus Virulence in the Drosophila Larval Model. *MBio* **12**,
1051 e0027621.
1052 **Ryu, J. H., Ha, E. M., Oh, C. T., Seol, J. H., Brey, P. T., Jin, I., Lee, D. G., Kim, J., Lee, D. and Lee, W. J.**
1053 (2006). An essential complementary role of NF-kappaB pathway to microbicidal oxidants in Drosophila
1054 gut immunity. *EMBO J* **25**, 3693-701. Epub 2006 Jul 20.
1055 **Stenbak, C. R., Ryu, J. H., Leulier, F., Pili-Floury, S., Parquet, C., Hervé, M., Chaput, C., Boneca, I. G.,**
1056 **Lee, W. J., Lemaitre, B. et al.** (2004). Peptidoglycan molecular requirements allowing detection by the
1057 Drosophila immune deficiency pathway. *J Immunol* **173**, 7339-48.
1058 **Storelli, G., Strigini, M., Grenier, T., Bozonnet, L., Schwarzer, M., Daniel, C., Matos, R. and Leulier, F.**
1059 (2018). Drosophila Perpetuates Nutritional Mutualism by Promoting the Fitness of Its Intestinal
1060 Symbiont Lactobacillus plantarum. *Cell Metab.* **27**, 362-377.e8. doi: 10.1016/j.cmet.2017.11.011. Epub
1061 2017 Dec 28.
1062 **Surendran, S., Huckesfeld, S., Waschle, B. and Pankratz, M. J.** (2017). Pathogen-induced food evasion
1063 behavior in Drosophila larvae. *J Exp Biol.* **220**, 1774-1780. doi: 10.1242/jeb.153395. Epub 2017 Mar 2.
1064 **Veenstra, J. A., Agricola, H. J. and Sellami, A.** (2008). Regulatory peptides in fruit fly midgut. *Cell Tissue*
1065 *Res* **334**, 499-516. doi: 10.1007/s00441-008-0708-3. Epub 2008 Oct 30.
1066 **Vodovar, N., Vinals, M., Liehl, P., Basset, A., Degrouard, J., Spellman, P., Boccard, F. and Lemaitre, B.**
1067 (2005). Drosophila host defense after oral infection by an entomopathogenic Pseudomonas species.
1068 *Proc Natl Acad Sci U S A* **102**, 11414-9. Epub 2005 Aug 1.
1069 **Wu, S. C., Liao, C. W., Pan, R. L. and Juang, J. L.** (2012). Infection-induced intestinal oxidative stress
1070 triggers organ-to-organ immunological communication in Drosophila. *Cell Host Microbe.* **11**, 410-7. doi:
1071 10.1016/j.chom.2012.03.004.
1072 **Younes, S., Al-Sulaiti, A., Nasser, E. A. A., Najjar, H. and Kamareddine, L.** (2020). Drosophila as a Model
1073 Organism in Host-Pathogen Interaction Studies. *Front Cell Infect Microbiol* **10**, 214.
1074 **Zhai, Z., Huang, X. and Yin, Y.** (2018). Beyond immunity: The Imd pathway as a coordinator of host
1075 defense, organismal physiology and behavior. *Dev Comp Immunol* **83**, 51-59.

1076

FIGURE 1

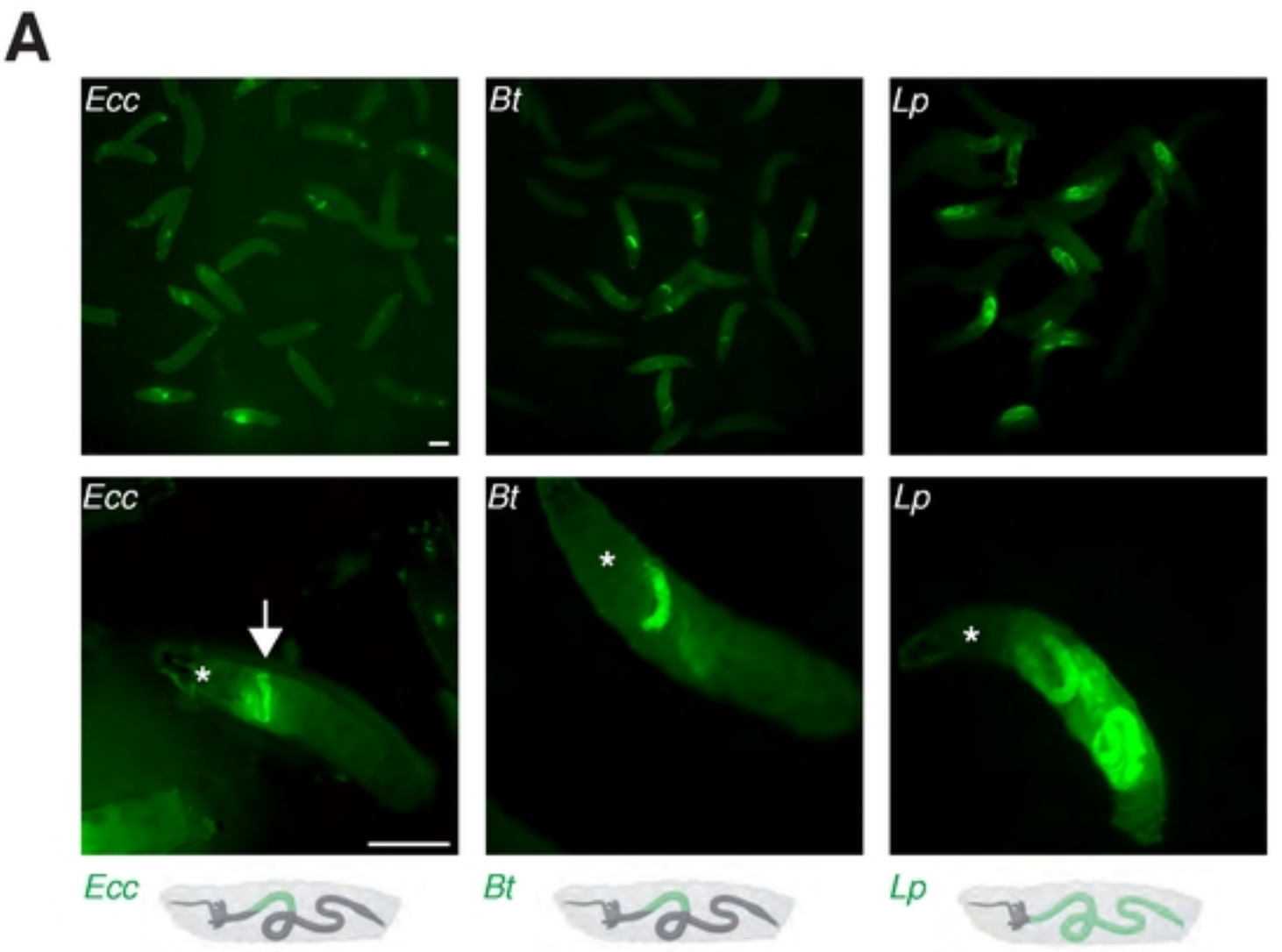
A
Ecc
Bt
Lp
Ecc
Bt
Lp
Ecc
Bt
Lp

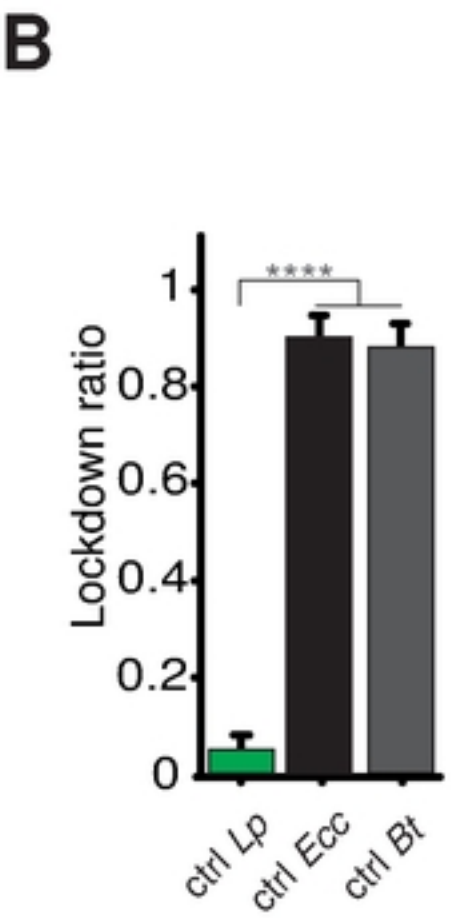
B
****
Lockdown ratio
1
0.8
0.6
0.4
0.2
0
ctrl Lp
ctrl Ecc
ctrl Bt

FIGURE 2

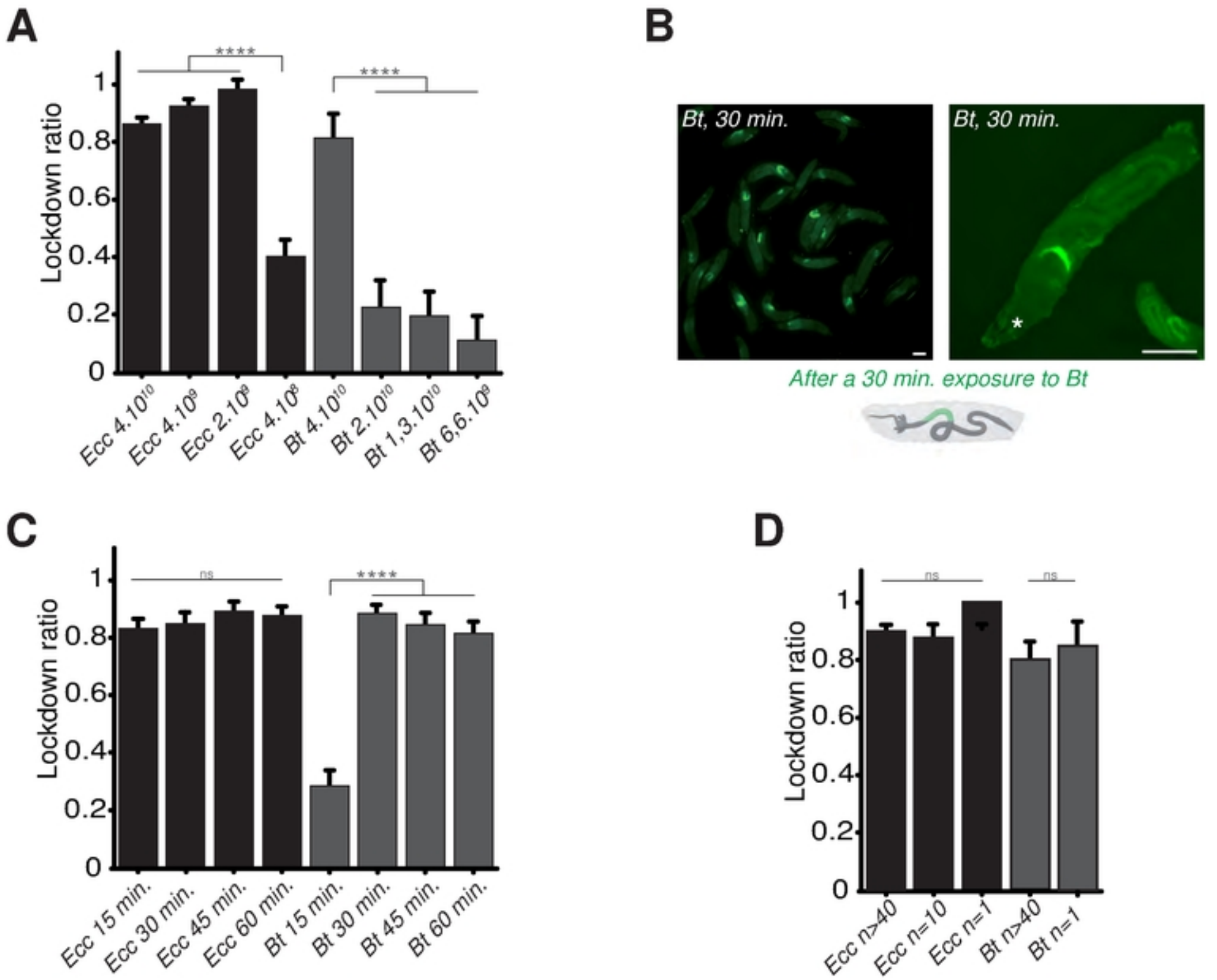
A
Lockdown ratio
****
****
Ecc 4.10^10
Ecc 4.10^9
Ecc 2.10^9
Ecc 4.10^8
Bt 4.10^10
Bt 2.10^10
Bt 1,3.10^10
Bt 6,6.10^9
B
Bt, 30 min.
Bt, 30 min.
After a 30 min. exposure to Bt
C
Lockdown ratio
ns
****
Ecc 15 min.
Ecc 30 min.
Ecc 45 min.
Ecc 60 min.
Bt 15 min.
Bt 30 min.
Bt 45 min.
Bt 60 min.
D
Lockdown ratio
ns
ns
Ecc n>40
Ecc n=10
Ecc n=1
Bt n>40
Bt n=1

FIGURE 3

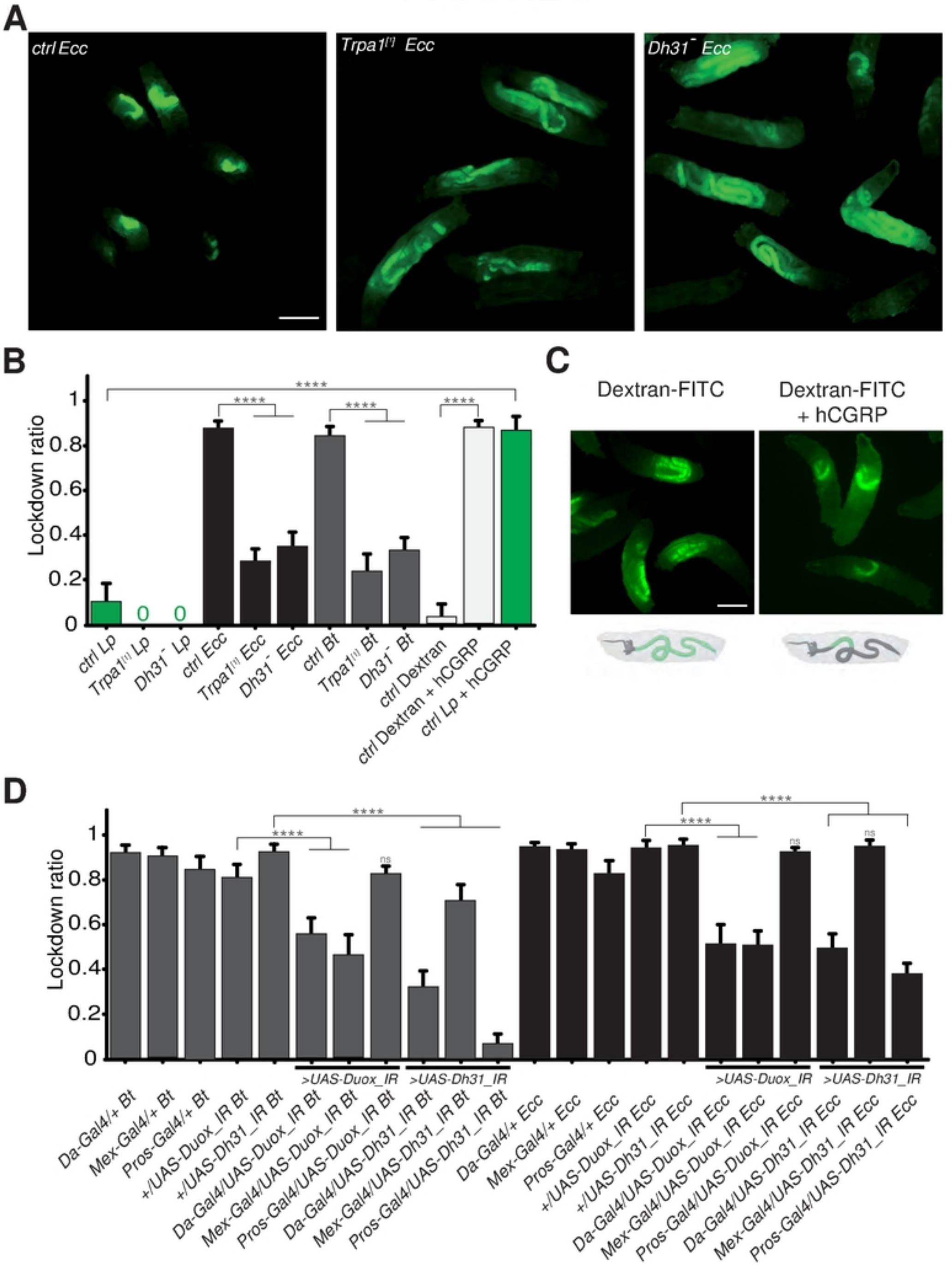
A
ctrl Ecc
Trpa1[1] Ecc
Dh31¯ Ecc
B
Lockdown ratio
1
0.8
0.6
0.4
0.2
0
****
0
0
ctrl Lp
Trpa1[1] Lp
Dh31¯ Lp
ctrl Ecc
Trpa1[1] Ecc
Dh31¯ Ecc
ctrl Bt
Trpa1[1] Bt
Dh31¯ Bt
ctrl Dextran
ctrl Dextran + hCGRP
ctrl Lp + hCGRP
C
Dextran-FITC
Dextran-FITC + hCGRP
D
Lockdown ratio
ns
>UAS-Duox_IR
>UAS-Dh31_IR
Da-Gal4/+ Bt
Mex-Gal4/+ Bt
Pros-Gal4/+ Bt
+/UAS-Duox_IR Bt
+/UAS-Dh31_IR Bt
Da-Gal4/UAS-Duox_IR Bt
Mex-Gal4/UAS-Duox_IR Bt
Pros-Gal4/UAS-Duox_IR Bt
Da-Gal4/UAS-Dh31_IR Bt
Mex-Gal4/UAS-Dh31_IR Bt
Pros-Gal4/UAS-Dh31_IR Bt
Da-Gal4/+ Ecc
Mex-Gal4/+ Ecc
Pros-Gal4/+ Ecc
+/UAS-Duox_IR Ecc
+/UAS-Dh31_IR Ecc
Da-Gal4/UAS-Duox_IR Ecc
Mex-Gal4/UAS-Duox_IR Ecc
Pros-Gal4/UAS-Duox_IR Ecc
Da-Gal4/UAS-Dh31_IR Ecc
Mex-Gal4/UAS-Dh31_IR Ecc
Pros-Gal4/UAS-Dh31_IR Ecc

FIGURE 4

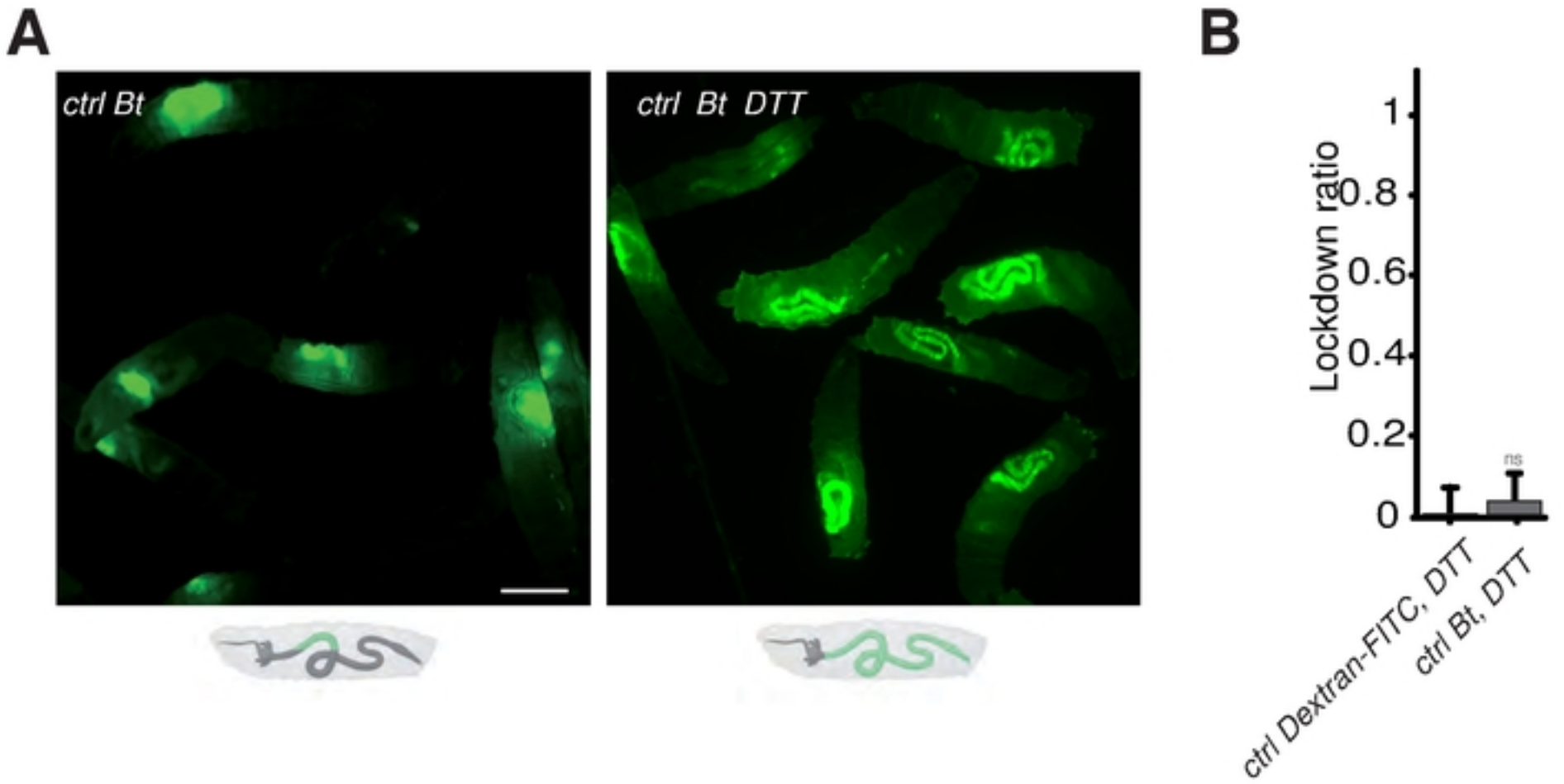
A
ctrl Bt
ctrl Bt DTT
B
Lockdown ratio
1
0.8
0.6
0.4
0.2
0
ns
ctrl Dextran-FITC, DTT
ctrl Bt, DTT

FIGURE 5

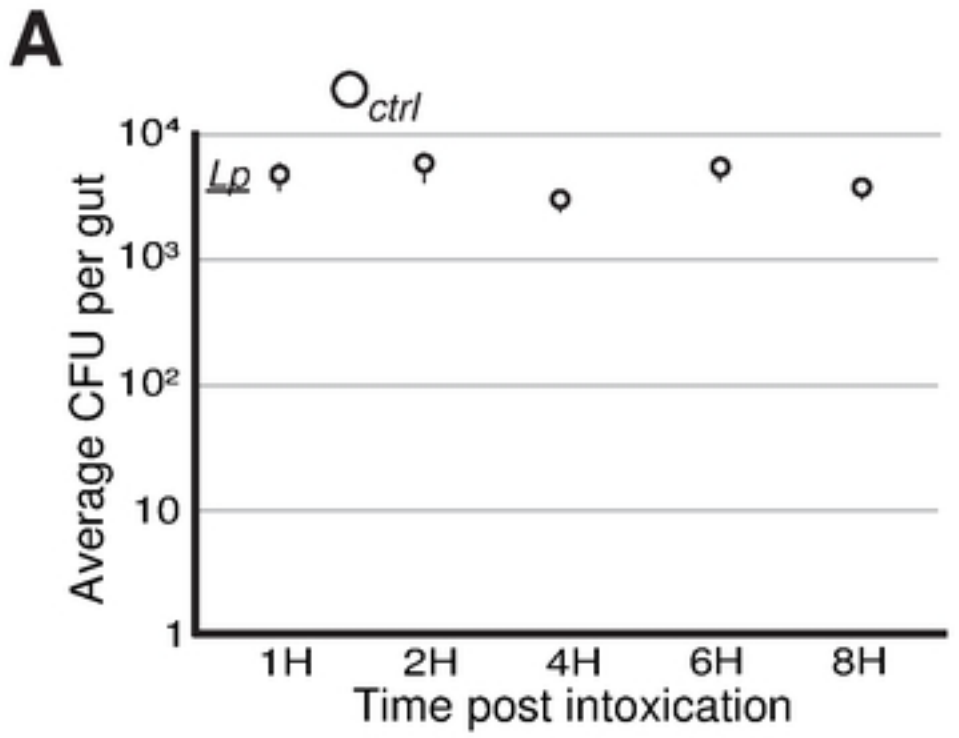
A
ctrl
Lp
Average CFU per gut
10^4
10^3
10^2
10
1
1H
2H
4H
6H
8H
Time post intoxication

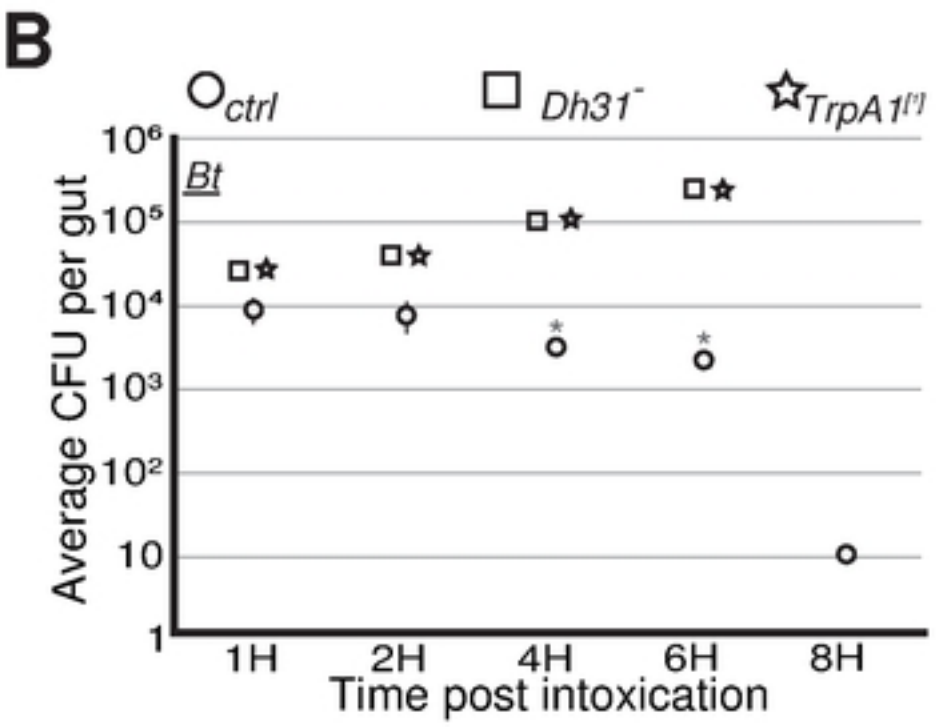
B
ctrl
Dh31⁻
TrpA1[1]
Bt
Average CFU per gut
10^6
10^5
10^4
10^3
10^2
10
1
1H
2H
4H
6H
8H
Time post intoxication

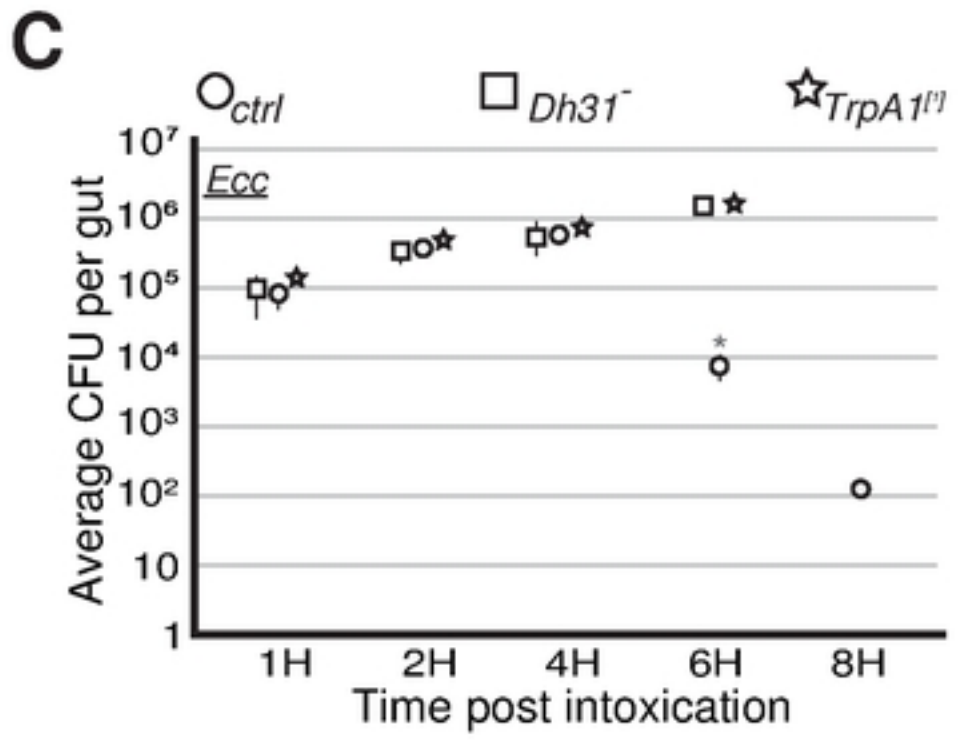
C
ctrl
Dh31⁻
TrpA1[1]
Ecc
Average CFU per gut
10^7
10^6
10^5
10^4
10^3
10^2
10
1
1H
2H
4H
6H
8H
Time post intoxication

D
ctrl Bt
TrpA1[1] Bt
Dh31⁻ Bt

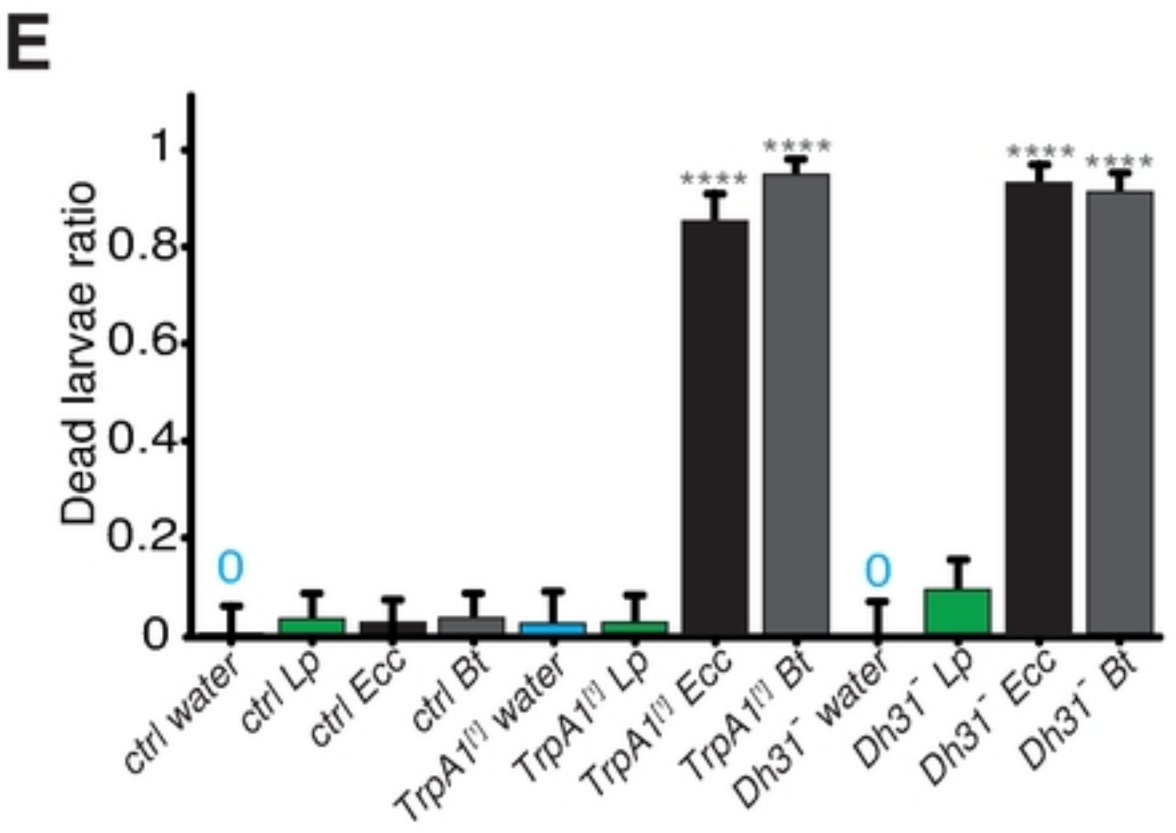
E
Dead larvae ratio
1
0.8
0.6
0.4
0.2
0
****
****
****
****
0
0
ctrl water
ctrl Lp
ctrl Ecc
ctrl Bt
TrpA1[1] water
TrpA1[1] Lp
TrpA1[1] Ecc
TrpA1[1] Bt
Dh31⁻ water
Dh31⁻ Lp
Dh31⁻ Ecc
Dh31⁻ Bt

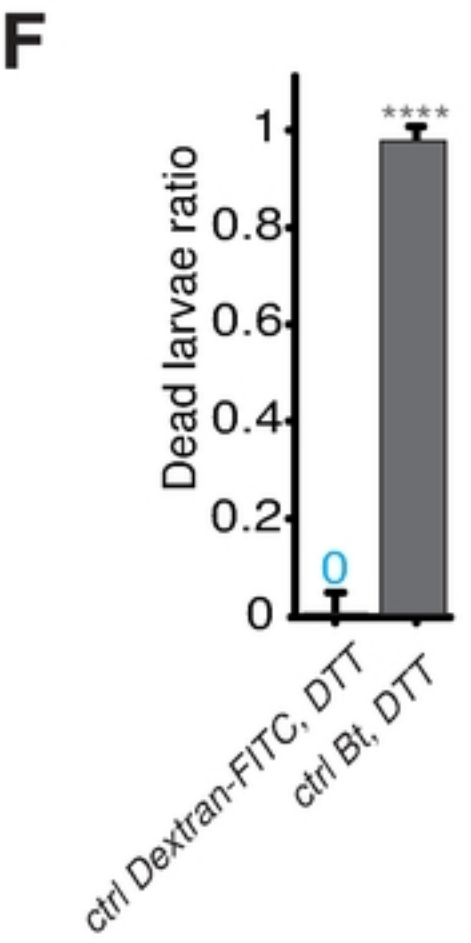
F
Dead larvae ratio
1
0.8
0.6
0.4
0.2
0
****
0
ctrl Dextran-FITC, DTT
ctrl Bt, DTT

FIGURE 6

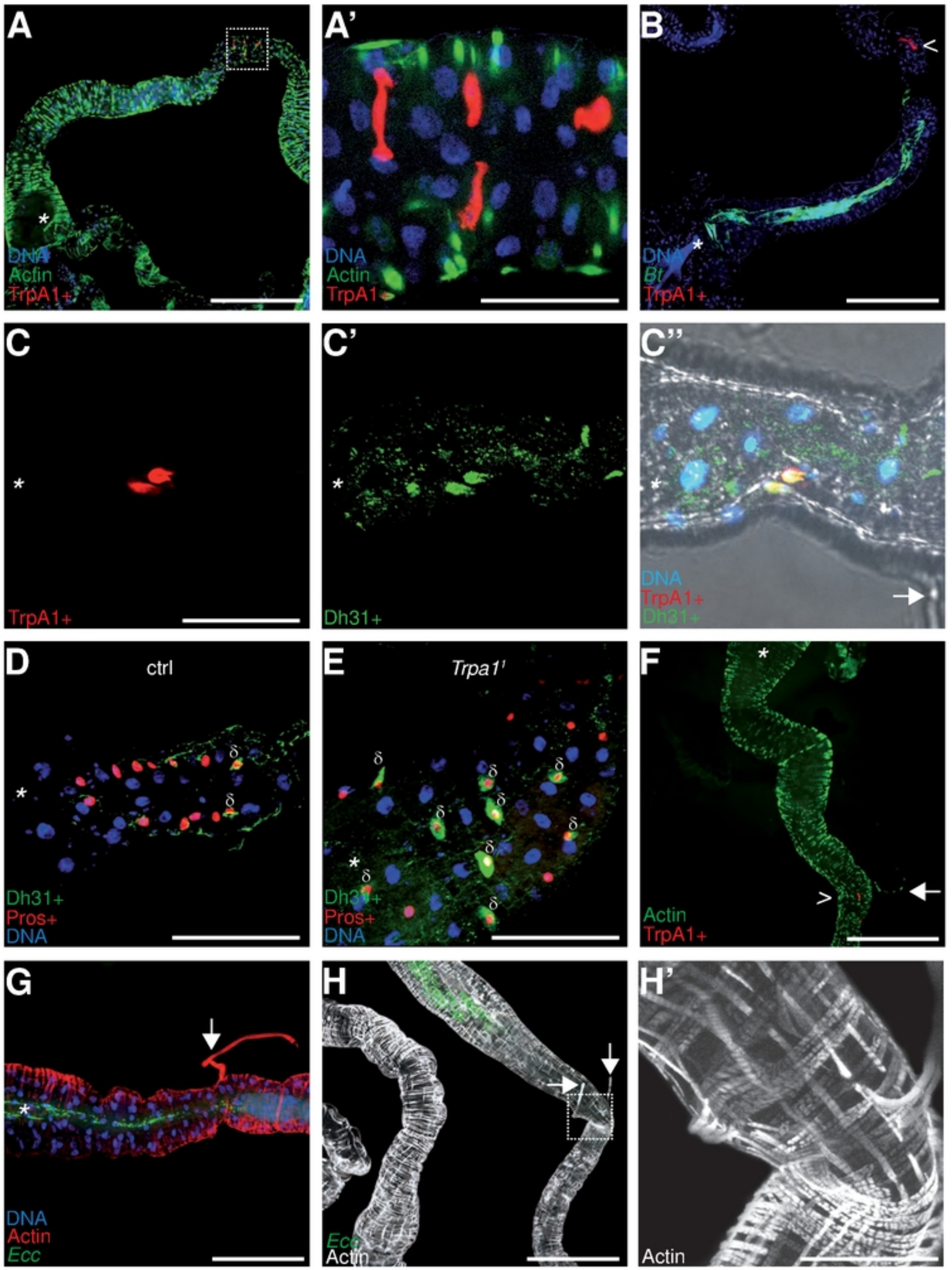
A
DNA
Actin
TrpA1+
A'
DNA
Actin
TrpA1+
B
DNA
Bt
TrpA1+
C
TrpA1+
C'
Dh31+
C''
DNA
TrpA1+
Dh31+
D
ctrl
Dh31+
Pros+
DNA
E
Trpa1¹
Dh31+
Pros+
DNA
F
Actin
TrpA1+
G
DNA
Actin
Ecc
H
Ecc
Actin
H'
Actin

FIGURE 7

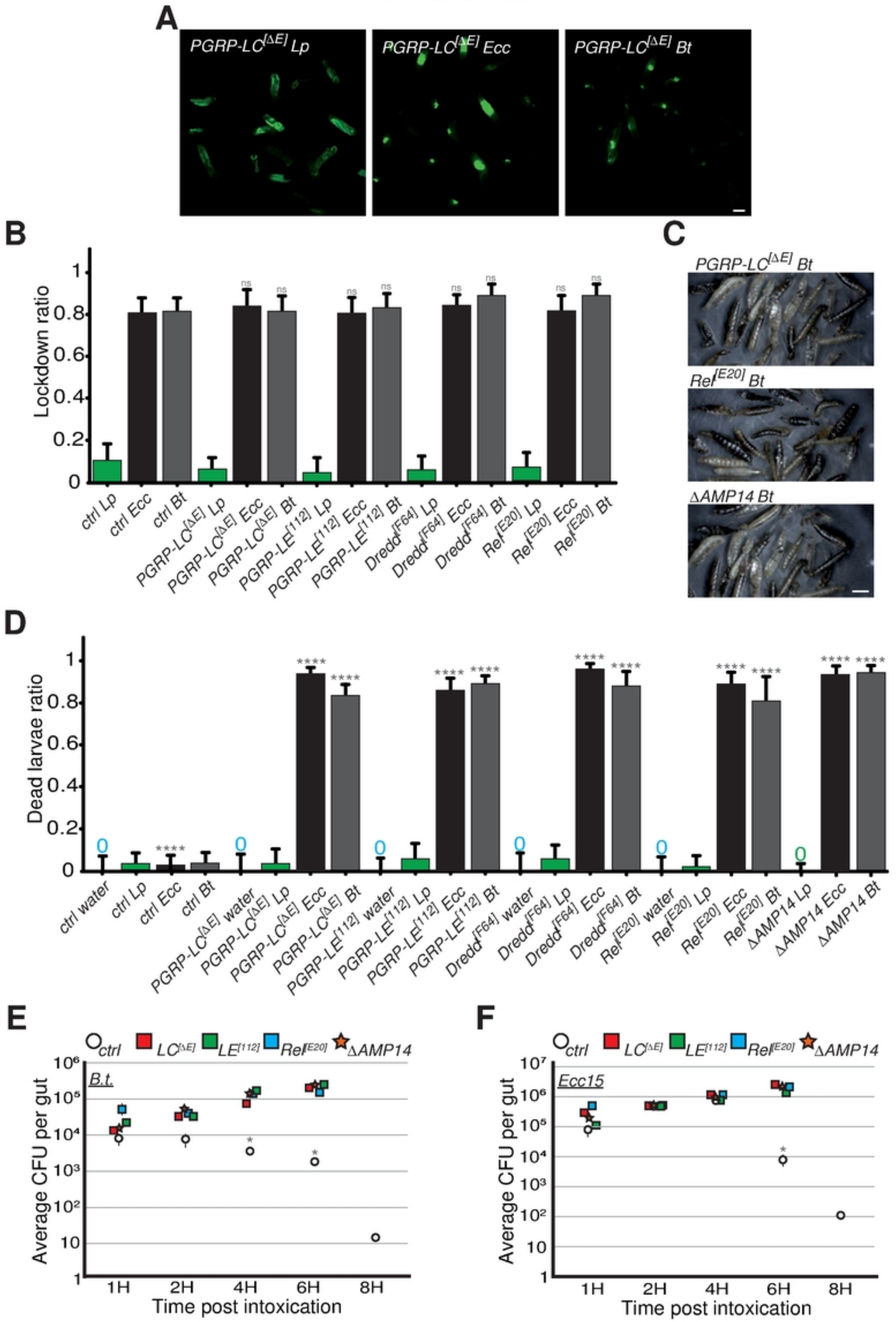
A
PGRP-LC[ΔE] Lp
PGRP-LC[ΔE] Ecc
PGRP-LC[ΔE] Bt
B
Lockdown ratio
ctrl Lp
ctrl Ecc
ctrl Bt
PGRP-LC[ΔE] Lp
PGRP-LC[ΔE] Ecc
PGRP-LC[ΔE] Bt
PGRP-LE[112] Lp
PGRP-LE[112] Ecc
PGRP-LE[112] Bt
Dredd[F64] Lp
Dredd[F64] Ecc
Dredd[F64] Bt
Rel[E20] Lp
Rel[E20] Ecc
Rel[E20] Bt
C
PGRP-LC[ΔE] Bt
Rel[E20] Bt
ΔAMP14 Bt
D
Dead larvae ratio
ctrl water
ctrl Lp
ctrl Ecc
ctrl Bt
PGRP-LC[ΔE] water
PGRP-LC[ΔE] Lp
PGRP-LC[ΔE] Ecc
PGRP-LC[ΔE] Bt
PGRP-LE[112] water
PGRP-LE[112] Lp
PGRP-LE[112] Ecc
PGRP-LE[112] Bt
Dredd[F64] water
Dredd[F64] Lp
Dredd[F64] Ecc
Dredd[F64] Bt
Rel[E20] water
Rel[E20] Lp
Rel[E20] Ecc
Rel[E20] Bt
ΔAMP14 Lp
ΔAMP14 Ecc
ΔAMP14 Bt
E
ctrl
LC[ΔE]
LE[112]
Rel[E20]
ΔAMP14
B.t.
Average CFU per gut
1H
2H
4H
6H
8H
Time post intoxication
F
Ecc15
Average CFU per gut
Time post intoxication

FIGURE 8

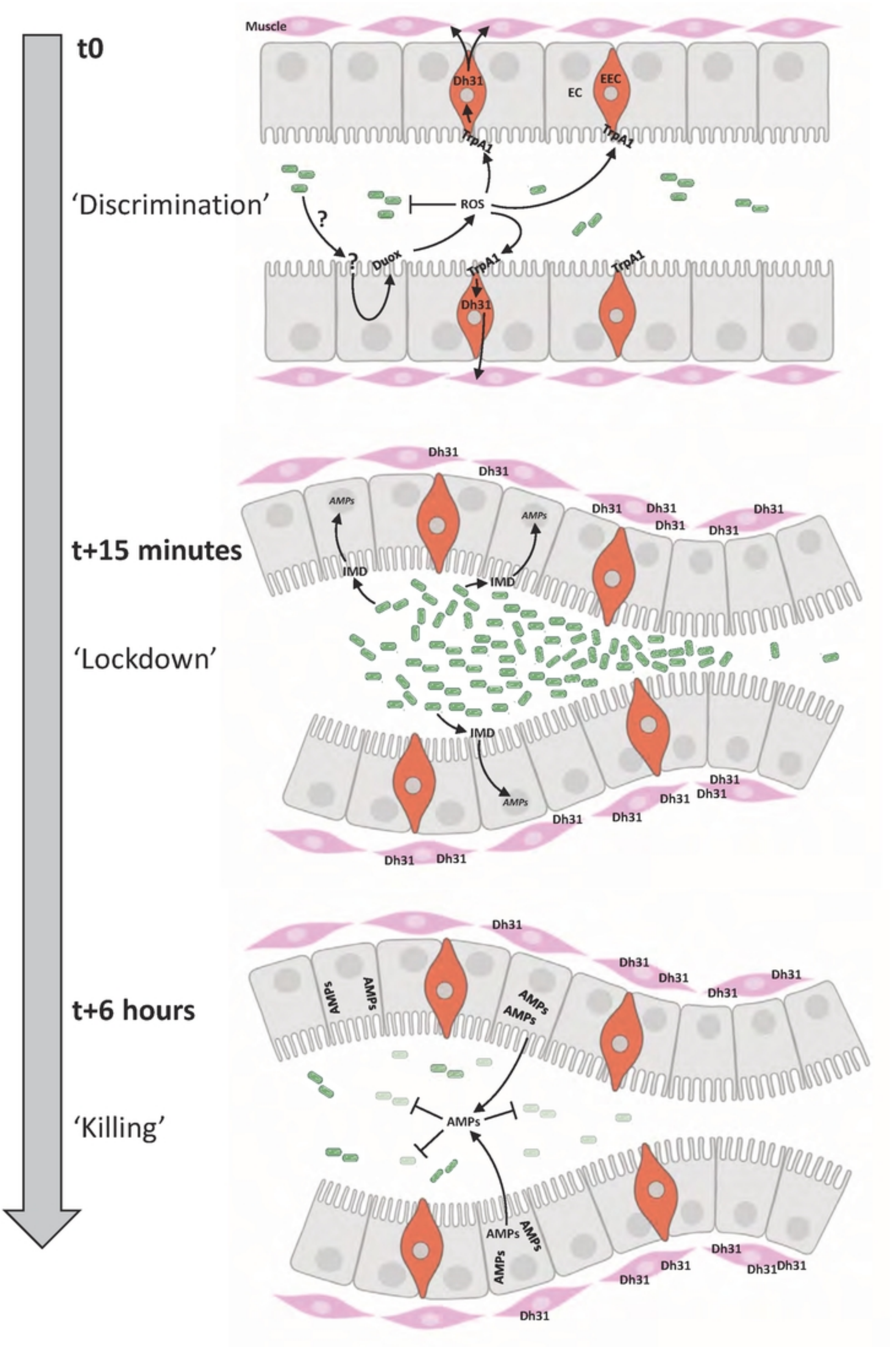
t0
'Discrimination'
Muscle
Dh31
EC
EEC
TrpA1
ROS
?
Duox
t+15 minutes
'Lockdown'
AMPs
IMD
t+6 hours
'Killing'

SUPP1

A

ctrl + *Ecc*

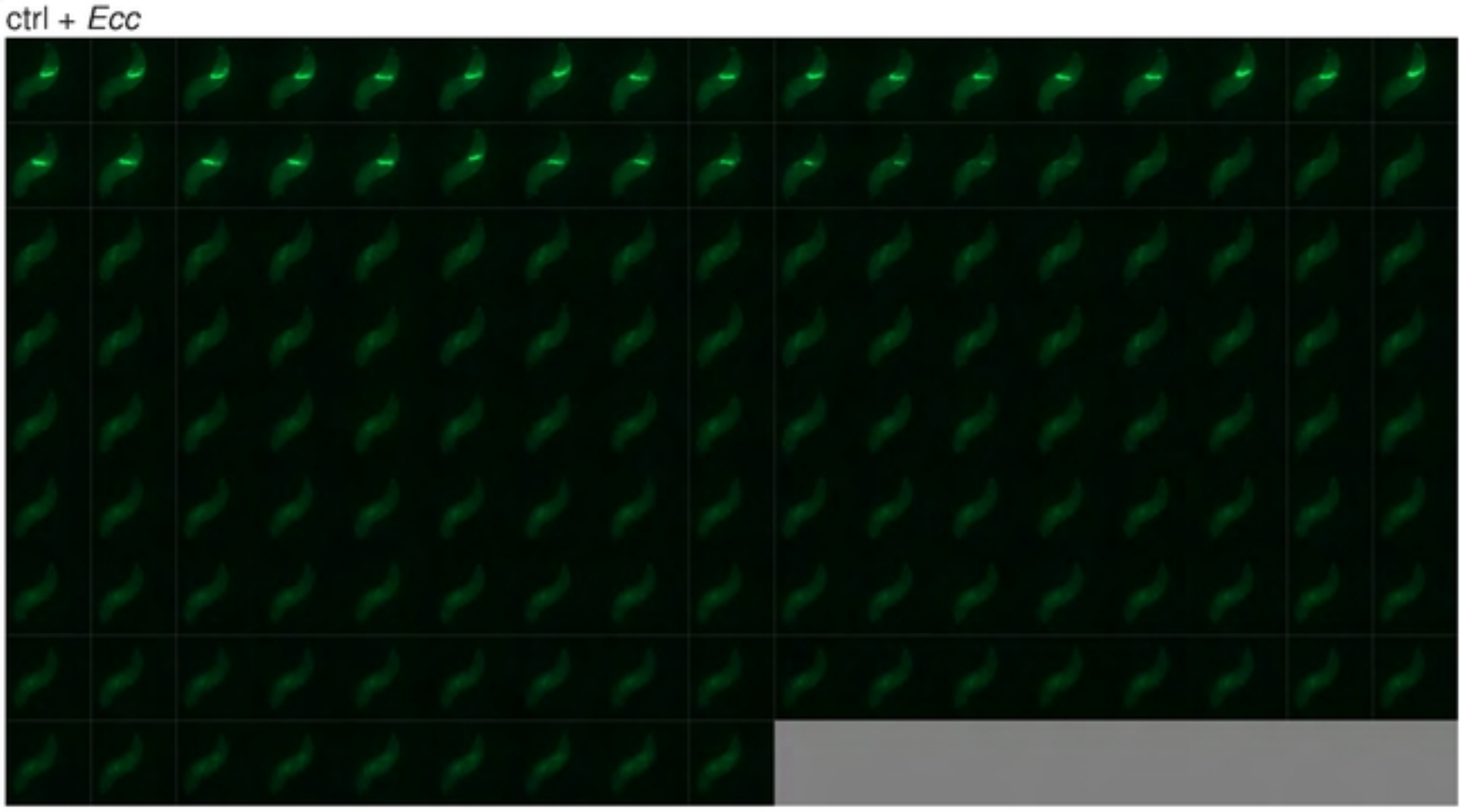

B

ctrl + *Bt*

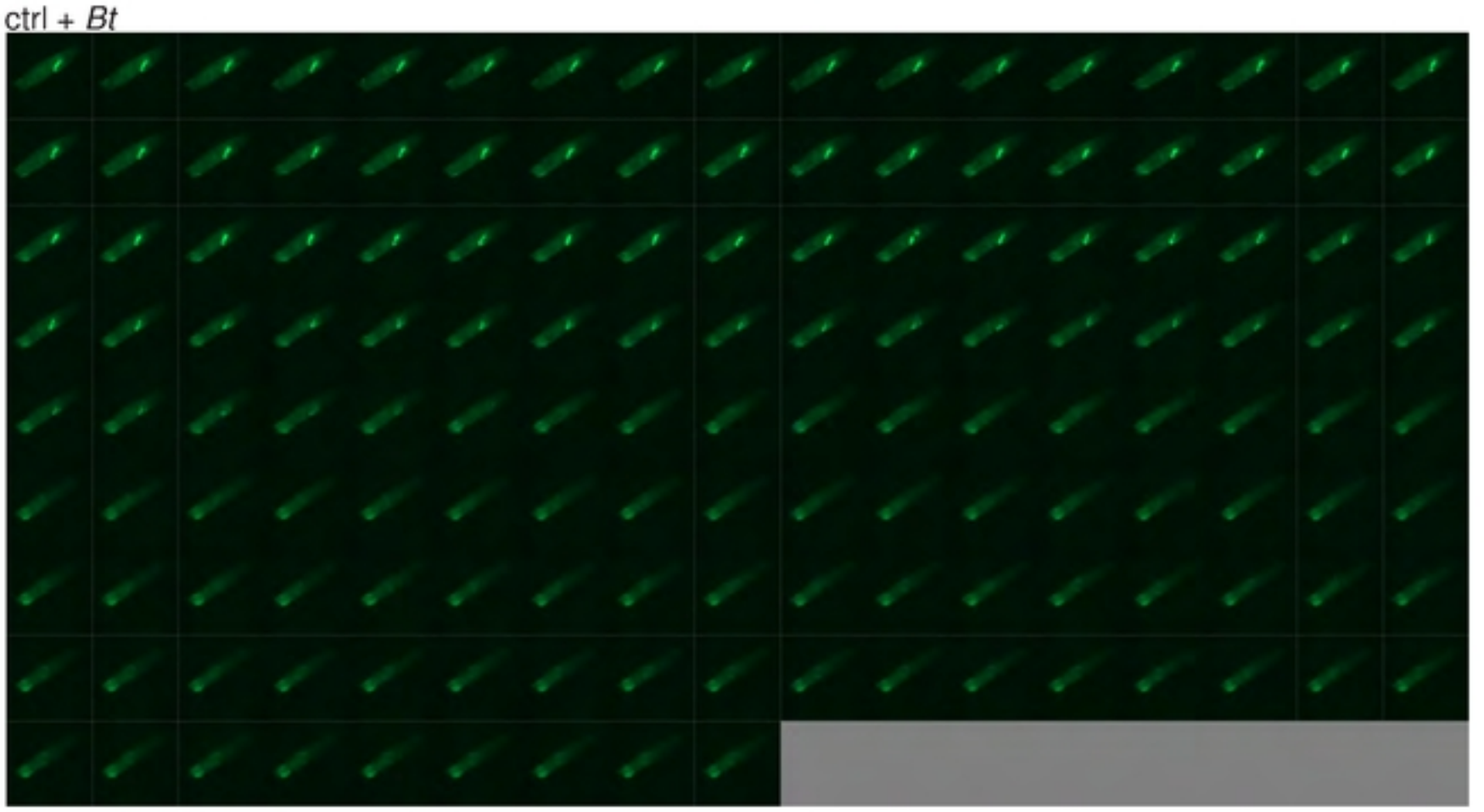

C

ctrl + *Lp*

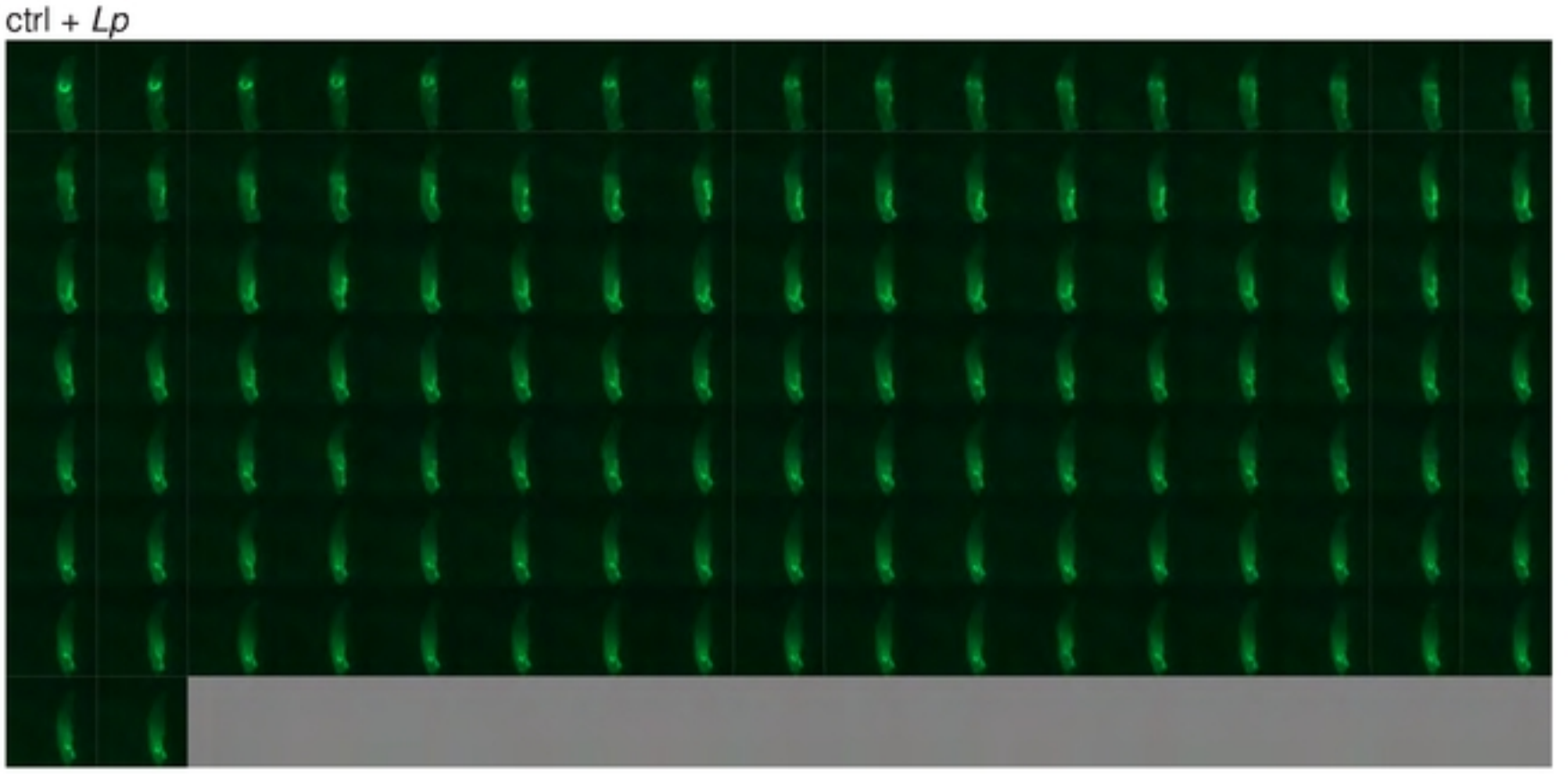

SUPP2

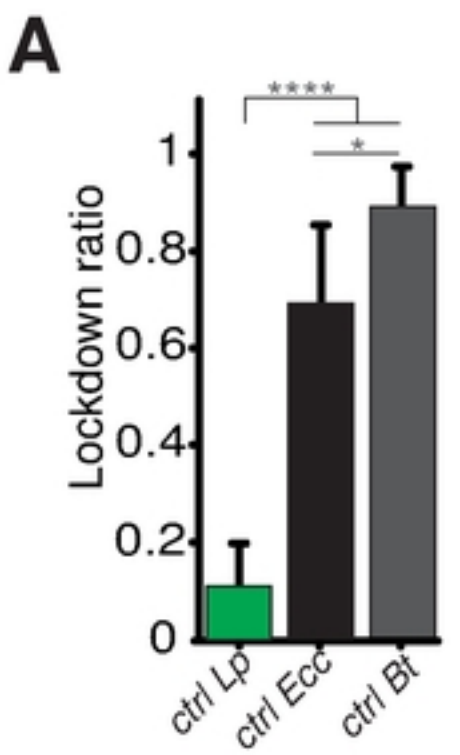

SUPP3

A

TrpA1[1] + *Ecc*

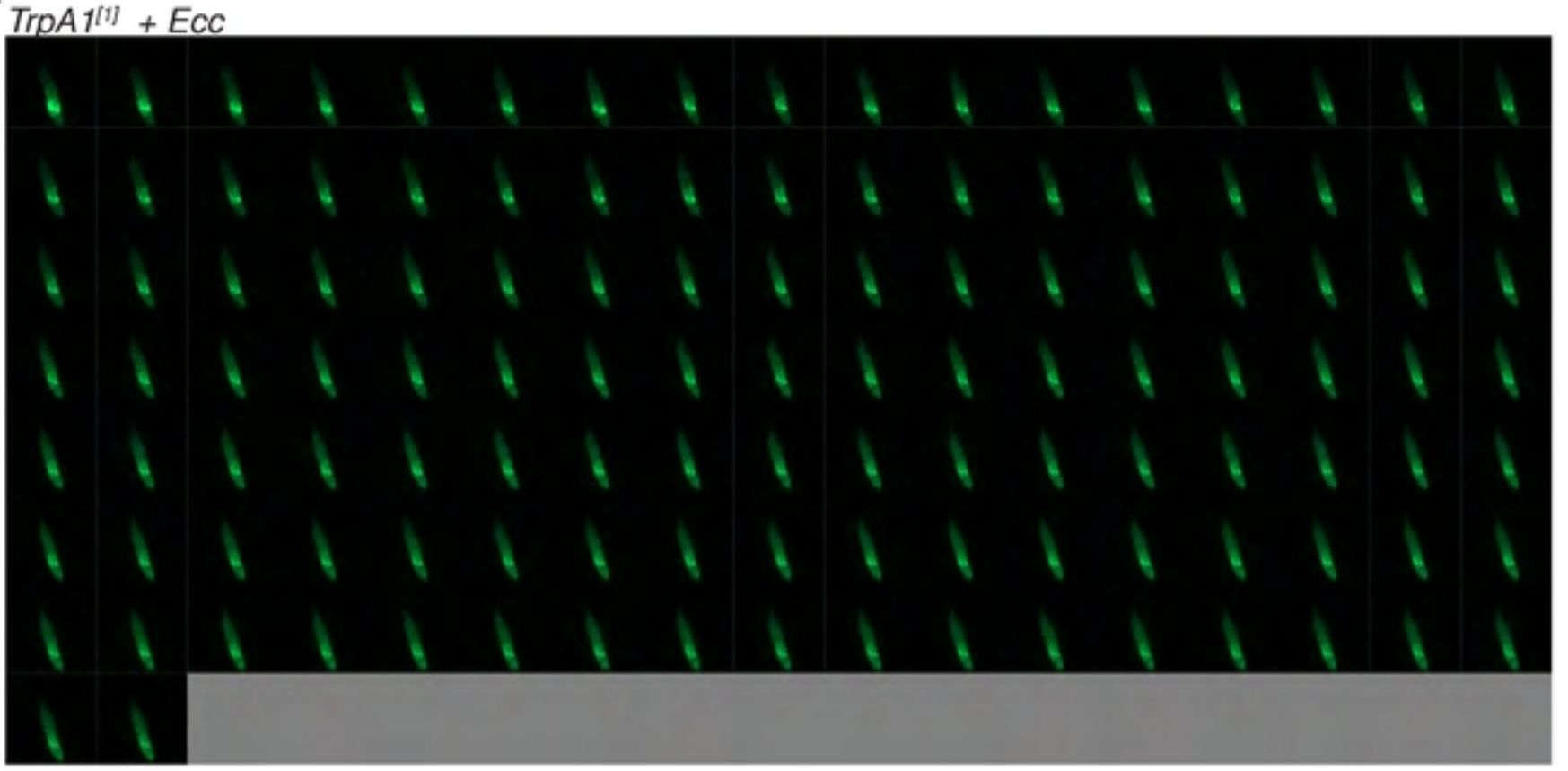

B

Dh31⁻ + *Ecc*

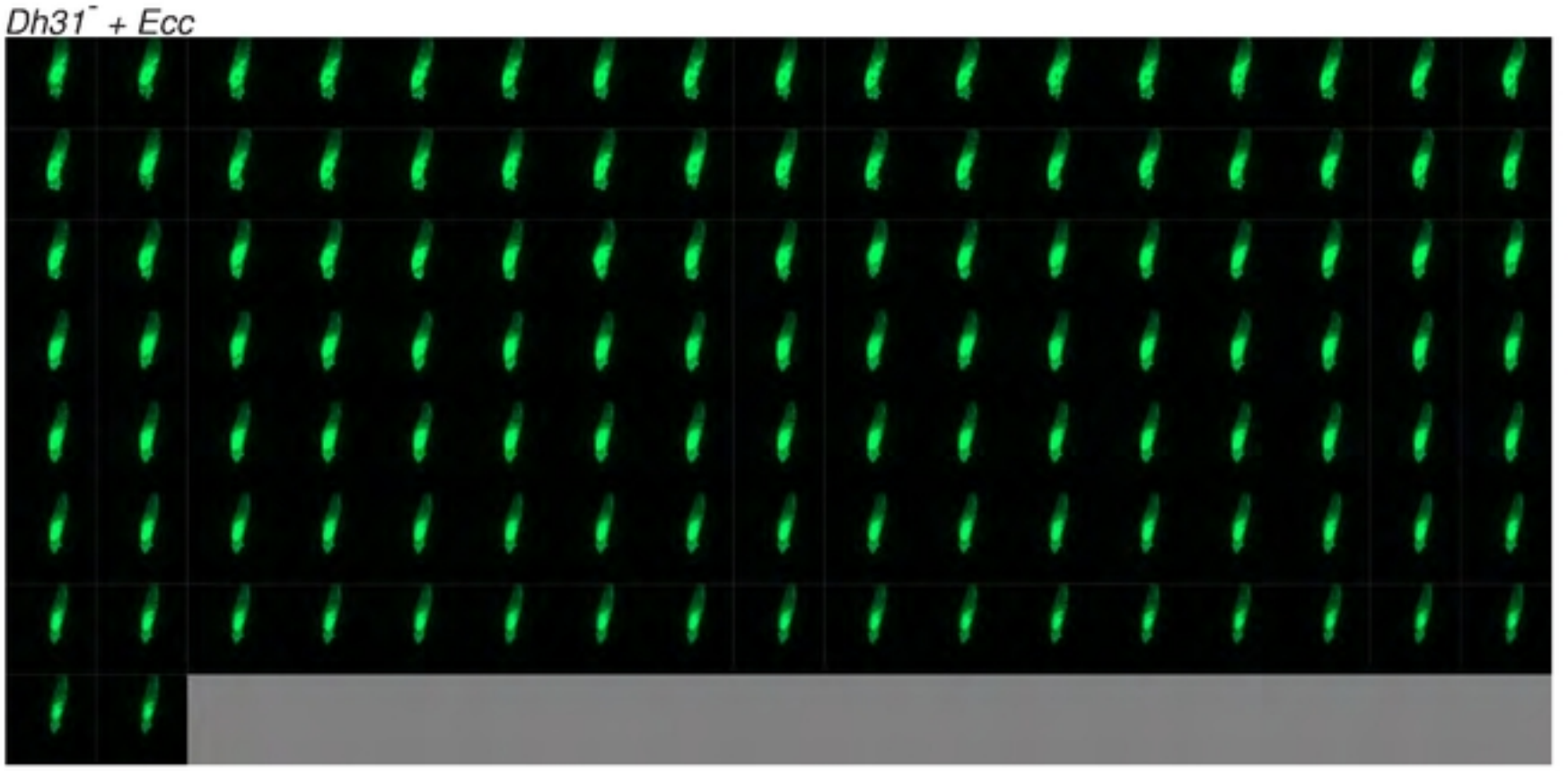

C

ctrl + *Lp* + hCGRP

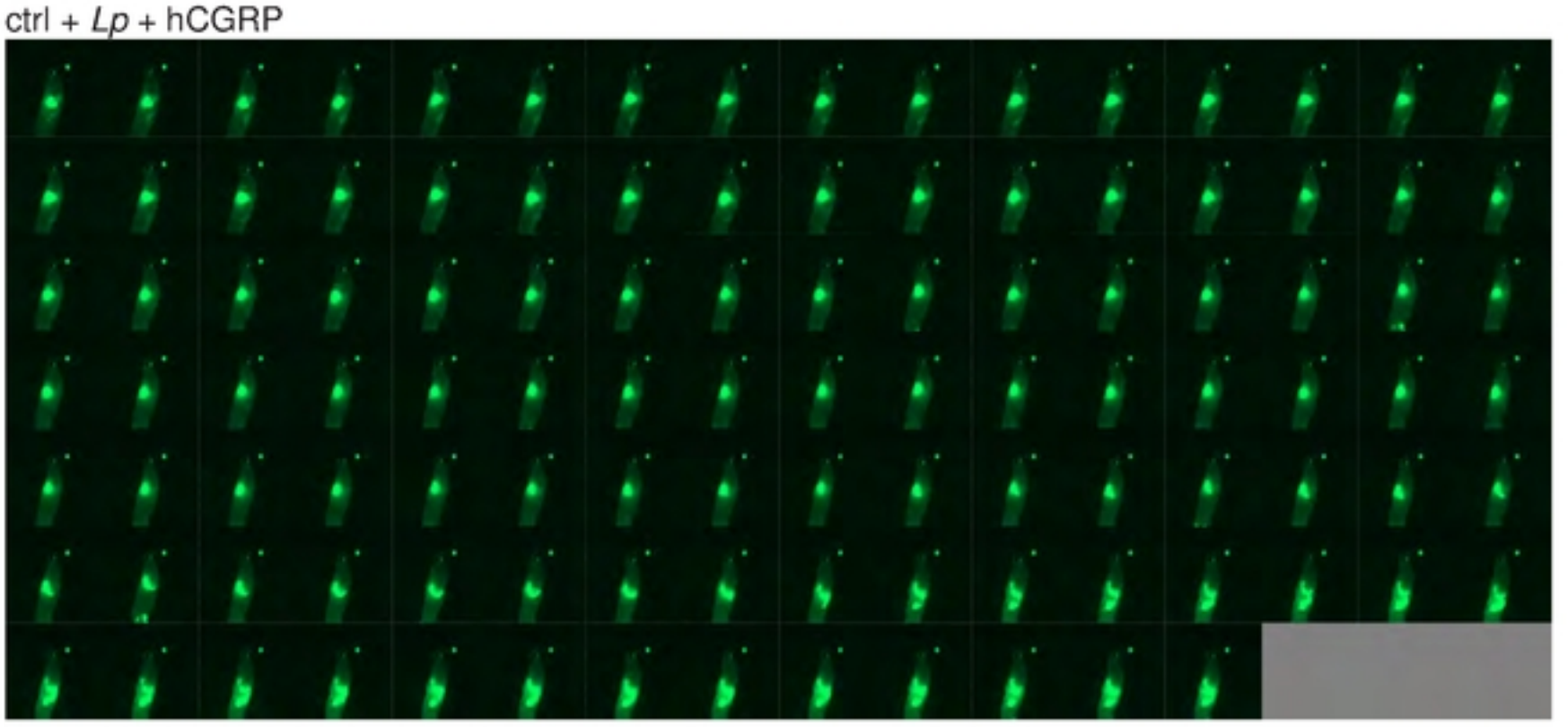

SUPP4

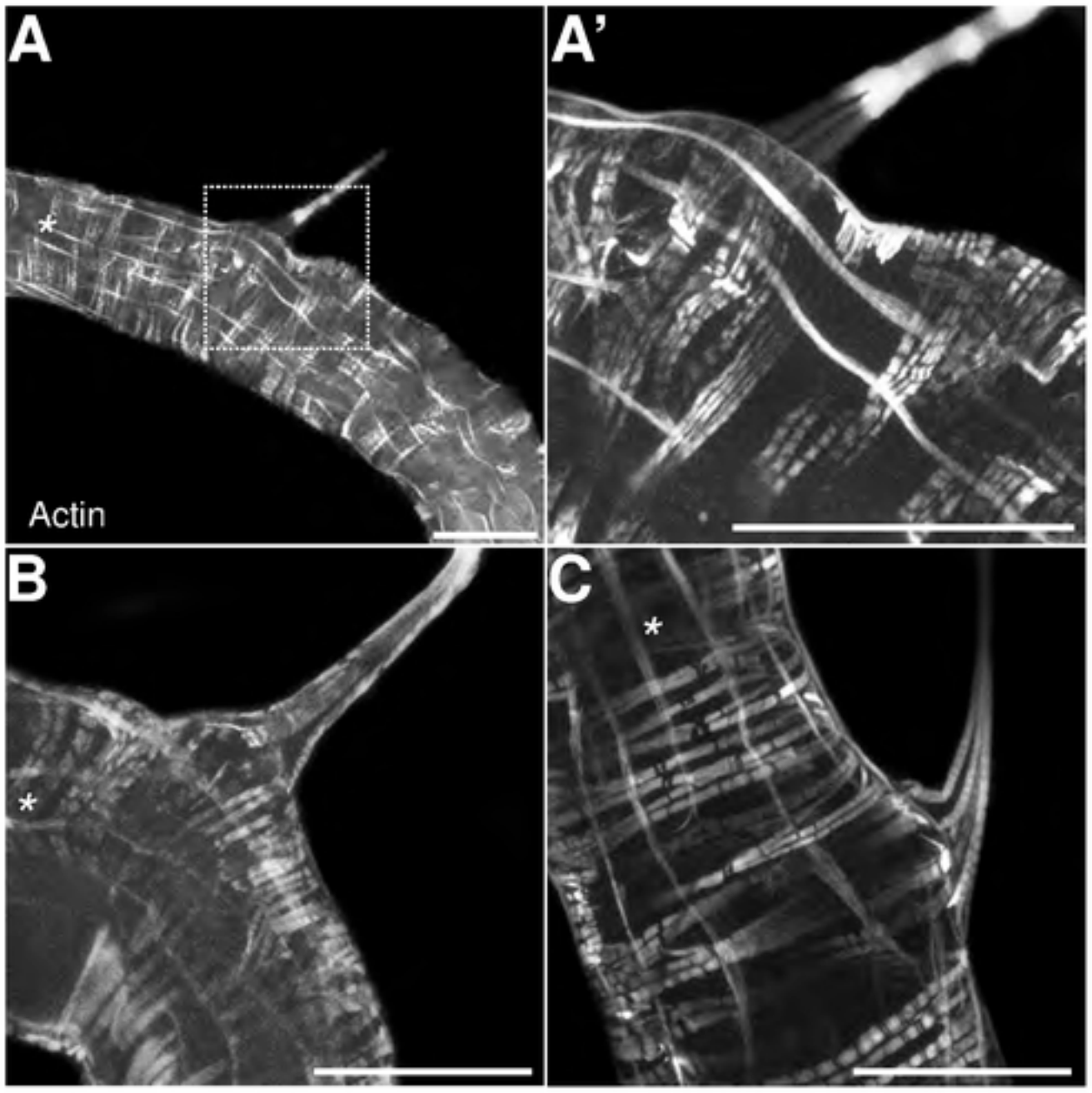

SUPP5

A *PGRP-LC$^{[\Delta E]}$ Bt*

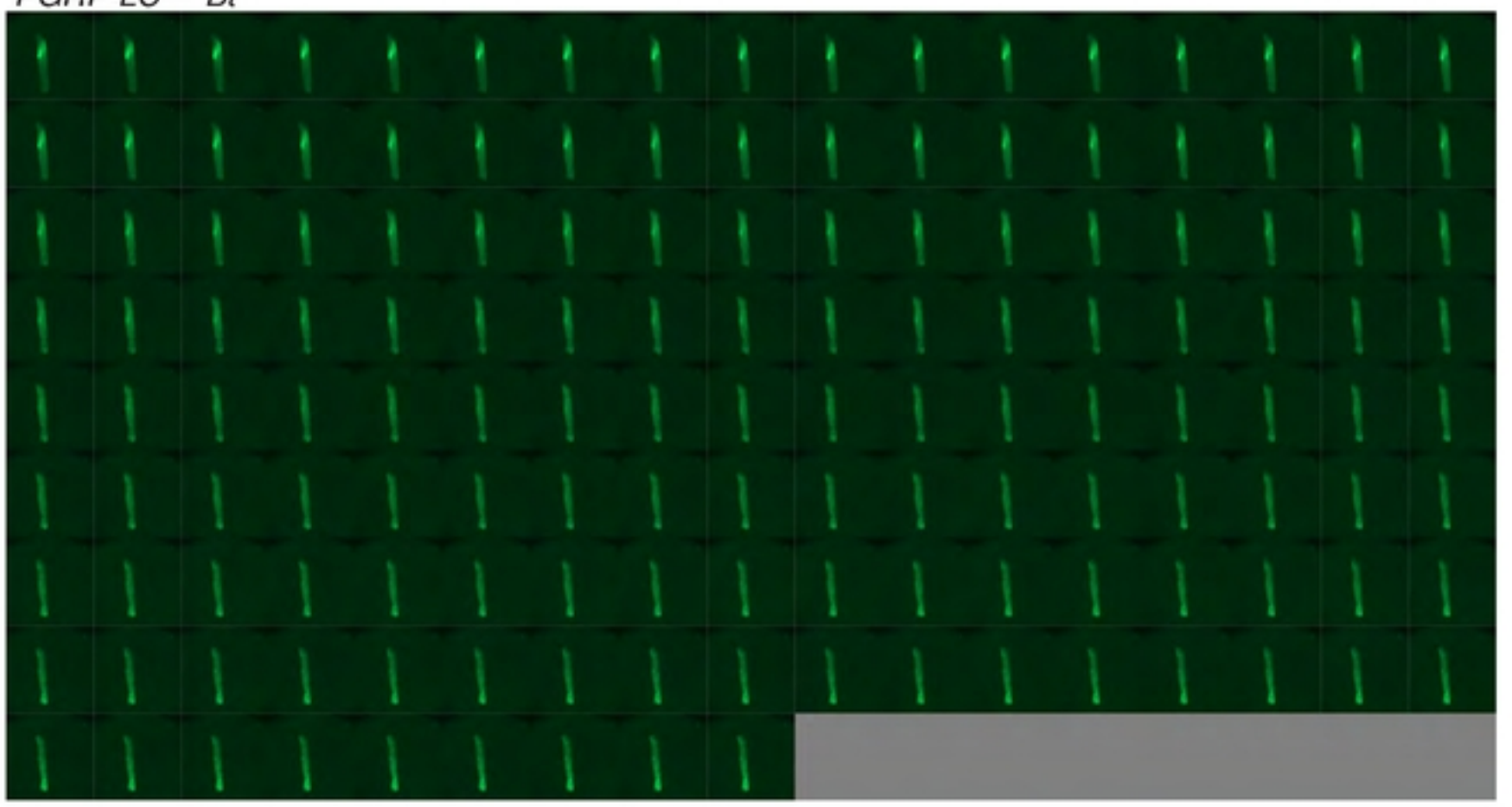

B *PGRP-LE$^{[112]}$ Ecc*

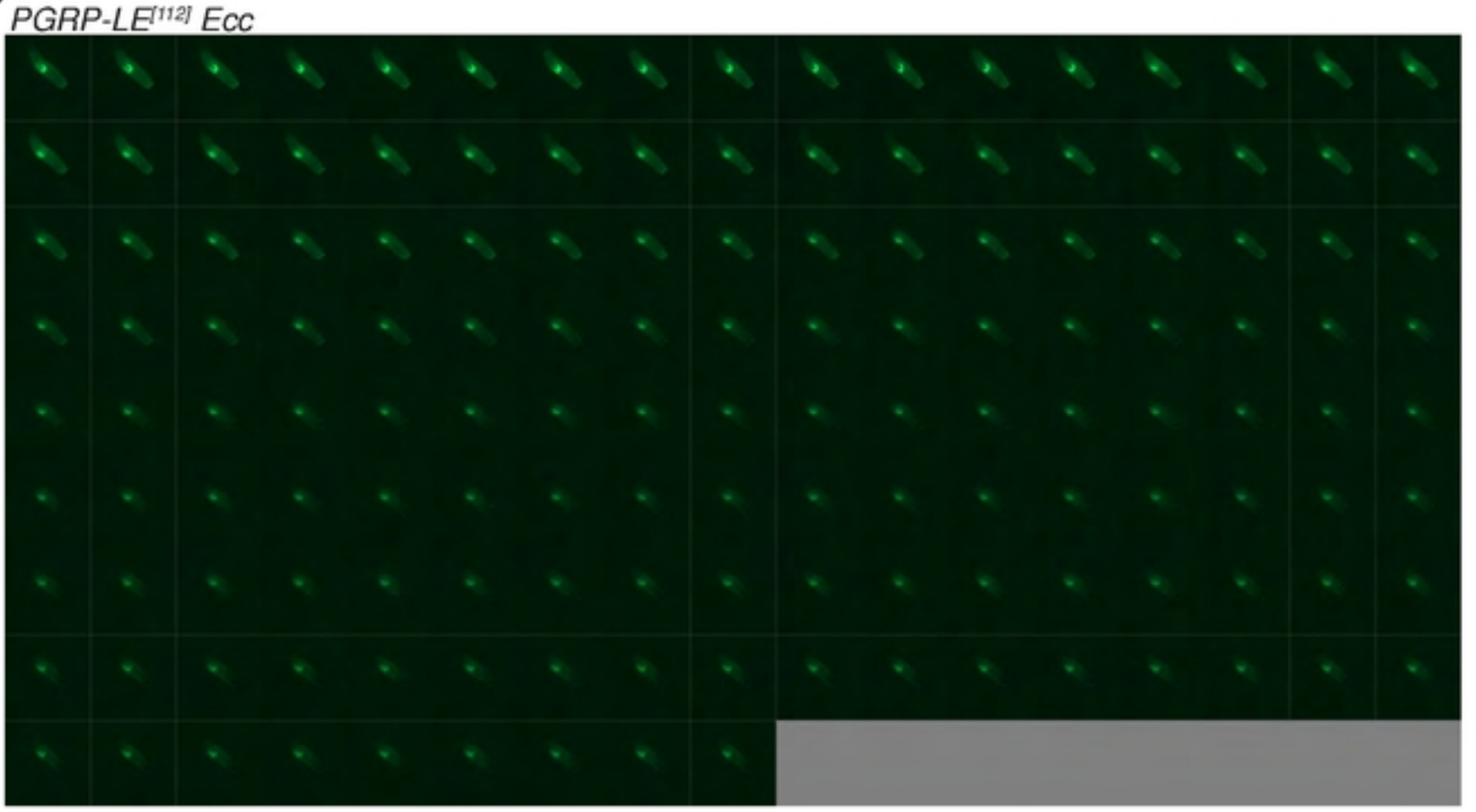
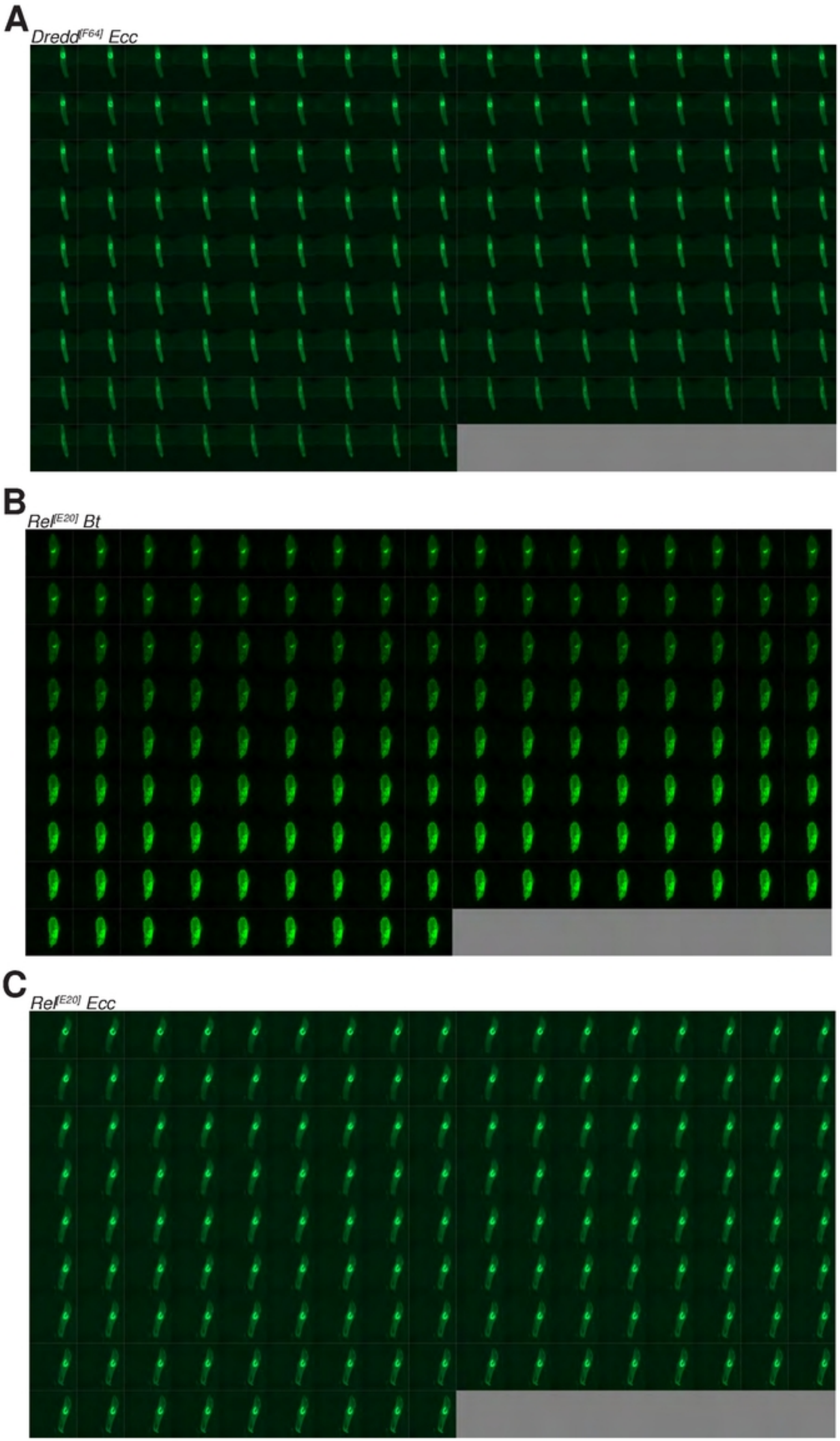
SUPP6